Available online at www.sciencedirect.com
ScienceDirect
Journal of Computational Physics 227 (2008) 4018–4037
JOURNAL OF COMPUTATIONAL PHYSICS
www.elsevier.com/locate/jcp

An effective explicit pressure gradient scheme implemented in the two-level non-staggered grids for incompressible Navier–Stokes equations

P.H. Chiu, Tony W.H. Sheu *, R.K. Lin

Department of Engineering Science and Ocean Engineering, National Taiwan University, No. 1, Sec. 4, Roosevelt Road, Taipei 106, Taiwan, ROC

Received 13 March 2007; received in revised form 13 July 2007; accepted 11 December 2007
Available online 23 December 2007

Abstract

In this paper, an improved two-level method is presented for effectively solving the incompressible Navier–Stokes equations. This proposed method solves a smaller system of nonlinear Navier–Stokes equations on the coarse mesh and needs to solve the Oseen-type linearized equations of motion only once on the fine mesh level. Within the proposed two-level framework, a prolongation operator, which is required to linearize the convective terms at the fine mesh level using the convergent Navier–Stokes solutions computed at the coarse mesh level, is rigorously derived to increase the prediction accuracy. This indispensable prolongation operator can properly communicate the flow velocities between the two mesh levels because it is locally analytic. Solution convergence can therefore be accelerated. For the sake of numerical accuracy, momentum equations are discretized by employing the general solution for the two-dimensional convection–diffusion–reaction model equation. The convective instability problem can be simultaneously eliminated thanks to the proper treatment of convective terms. The converged solution is, thus, very high in accuracy as well as in yielding a quadratic spatial rate of convergence. For the sake of programming simplicity and computational efficiency, pressure gradient terms are rigorously discretized within the explicit framework in the non-staggered grid system. The proposed analytical prolongation operator for the mapping of solutions from the coarse to fine meshes and the explicit pressure gradient discretization scheme, which accommodates the dispersion-relation-preserving property, have been both rigorously justified from the predicted Navier–Stokes solutions.

Keywords: Two-level method; Navier–Stokes equations; Prolongation operator; Convection–diffusion–reaction; Explicit pressure gradient discretization; Dispersion-relation-preserving

1. Introduction

Numerical simulation of incompressible viscous fluid flows remains an area of continuous challenges due to the approximation of advective terms in the multi-dimensional domain. In addition to the notorious

* Corresponding author. Tel.: +886 2 33665791; fax: +886 2 23929885.
E-mail address: twhsheu@ntu.edu.tw (T.W.H. Sheu).

0021-9991/$ - see front matter © 2007 Elsevier Inc. All rights reserved.
doi:10.1016/j.jcp.2007.12.007

convective instability problem, approximation of these direction relevant terms can introduce false diffusion error [1]. Therefore, a well-suited multi-dimensional upwinding scheme should effectively dispense with the crosswind diffusion error without at the sacrifice of scheme destabilization. Splitting of the equation has been known to be a proper way to solve the multi-dimensional equation by obtaining the solutions more efficiently and accurately using the analytical one-dimensional model [2]. We propose in this paper, however, a truly two-dimensional flux discretization scheme to avoid slow convergence in the operator sweeping. To reduce the afore-mentioned false diffusion error, the general solution of the investigated two-dimensional model transport equation will be taken into account in the approximation of flux terms for velocities.

When simulating the steady incompressible Navier–Stokes equations in co-located (or non-staggered) grids, node-to-node oscillatory pressure solutions arising from the decoupling of velocity and pressure fields have been frequently reported [1]. This motivated us to discretize the currently investigated elliptic-type partial differential equations within the non-staggered grid context to prevent the oscillatory pressure solutions. When solving the incompressible Navier–Stokes in non-staggered grids, central approximation of the pressure gradient terms may lead to pressure odd–even decoupling. In order to eliminate this problem, an adequate amount of artificial dampings can be added to the scheme implicitly or explicitly for the sake of stability enhancement [3–6].

Linearization of the nonlinear terms in the incompressible Navier–Stokes equations plays another essential role in the assessment of computational efficiency. Improper linearization of convection terms in the flow equations may slow down convergence or can even cause the divergent solution to occur. Amongst the methods reported in the literature for the linearization of nonlinear Navier–Stokes equations, the multi-level method has gained an increasing acceptance in the past few years. As the name of this class of methods indicates, the multi-level method [7,8] involves calculating the solutions at different levels of the grid system. Take the two-level method as an example, the differential equation is solved firstly at nodes in the coarse grid system, at which the solutions can be computed less expensively. This is followed by a computationally more intensive calculation of the same differential equation on the fine mesh. Note that the convergent solutions must be calculated in the coarse mesh. As a result, the linearization method chosen for the convective terms shown in the momentum equation plays also an essential role. For this reason, the computationally more efficient Oseen-type linearization method will be employed to render the linearized equation cast in the convection–diffusion–reaction differential form.

The reminder of this paper is organized as follows. In Section 2, the governing equations cast in the primitive variable form are solved along with the prescribed pressure boundary value. This is followed by presenting the proposed prolongation operator for effectively mapping the convergent solutions obtained at the coarse mesh to those obtained at the fine mesh. In Section 4, the underlying five-point convection–diffusion–reaction (CDR) scheme will be presented to accurately solve the linearized momentum transport equations. Two theoretically derived discrete pressure gradient operators are also presented in Section 4 in order to save the CPU time without suffering from even–odd oscillations in the non-staggered grids. In Section 5, the two-level Oseen model implemented with the proposed implicit and explicit compact pressure gradient approximation schemes is analytically validated by solving the problem which is amenable to the exact solution. Finally, some conclusions are drawn in Section 6.

2. Governing equations

The incompressible viscous flow motion, which is governed by the following continuity and momentum equations, will be dealt with in this paper:

$$\nabla \cdot \mathbf{u} = 0, \tag{1}$$

$$(\mathbf{u} \cdot \nabla)\mathbf{u} = -\nabla p + \frac{1}{Re}\nabla^2 \mathbf{u} + \mathbf{f}. \tag{2}$$

The chosen primitive variables $(\mathbf{u}, p)$ will be sought subject solely to the specified boundary condition for $\mathbf{u}$ [9]. All lengths have been normalized by L, the velocity components by u_∞, the time by L/u_∞, and the pressure by ρu_∞^2, where ρ denotes the fluid density. The resulting Reynolds number Re $(\equiv \rho u_\infty L/\mu)$ represents the measure of equation nonlinearity.

Momentum conservation equations can be solved together with the divergence-free constraint equation for the velocity (or continuity equation) to preserve the fluid flow incompressibility. The eigenvalue distribution of the resulting coupled system of matrix equations can become, however, fairly ill-conditioned. It is, therefore, very difficult to calculate the solutions $(\mathbf{u}, p)$ from (1) and (2) using some computationally less expensive iterative solvers [10]. Calculation of the matrix equations may exceed the computer power and disk space. The above two drawbacks make the coupled formulation infeasibly to be applied. One way of overcoming the afore-mentioned difficulty is to apply the well-known pressure Poisson equation (PPE) approach [11]. By applying a curl operator on each momentum equation, the Poisson equation for the pressure p can be derived in lieu of the divergence-free equation (1) as

$$\nabla^2 p = \nabla \cdot \left[-(\mathbf{u} \cdot \nabla)\mathbf{u} + \frac{1}{Re}\nabla^2 \mathbf{u} + \mathbf{f} \right]. \tag{3}$$

Application of segregated approach should be subject to the integral condition for the pressure [9]. Our current aim is to refine the Navier–Stokes solver without the involvement of a computationally more challenging integral condition. We specify, therefore, in this study the conventional Neumann-type boundary condition $\frac{\partial p}{\partial n} = [-(\mathbf{u} \cdot \nabla)\mathbf{u} + \frac{1}{Re}\nabla^2 \mathbf{u} + \mathbf{f}] \cdot \mathbf{n}$ [11], where $\mathbf{n}$ denotes the unit outward vector normal to the boundary of the investigated physical domain.

3. Two-level Navier–Stokes solver

In this section, the linearization method for the convective term $(\underline{u} \cdot \nabla)\underline{u}$ will be presented in both coarse and fine meshes. Within the Newton linearization framework, expansion of ST with respect to the two arbitrary variables S and T at the iteration level k leads to the following updated expression for ST, namely, $S^{k+1}T^{k+1} = S^{k+1}T^k + S^k T^{k+1} - S^k T^k + \cdots + \text{H.O.T.}$ By virtue of this expansion equation, $(u^2)_x^{k+1}$ and $(uv)_y^{k+1}$ shown in the x- and y-momentum equations can be approximated to render the following two Newton linearized momentum equations (2) along the x- and y-directions, respectively:

$$u^k u_x^{k+1} + v^k u_y^{k+1} - \frac{1}{Re}\nabla^2 u^{k+1} + \underline{u_x^k u^{k+1}} = -p_x^{k+1} + \underline{u^k u_x^k + v^k u_y^k - u_y^k v^{k+1}}, \tag{4}$$

$$u^k v_x^{k+1} + v^k v_y^{k+1} - \frac{1}{Re}\nabla^2 v^{k+1} + \underline{v_y^k v^{k+1}} = -p_y^{k+1} + \underline{u^k v_x^k + v^k v_y^k - v_x^k u^{k+1}}. \tag{5}$$

The underlined terms shown above represent the high-order correction terms to the classical frozen-coefficient linearized equations.

The convective terms in Eqs. (4) and (5) are known to be the origin of scheme instability, which will be suppressed by applying the upwinding convective scheme described later. The matrix indefiniteness owing to the reaction (or production) term $\nabla \mathbf{u}^k \cdot \mathbf{u}^{k+1}$ may also destabilize the discrete equation [12]. For this reason, the potentially destabilizing positive-valued reaction terms shown in the Newton linearized equations (4) and (5) have been omitted for the sake of stability. The resulting modified Picard (or Oseen-type) linearization method is, therefore, regarded as the simplified Newton linearization method. The enhanced matrix definiteness explains why the Oseen-type linearization method is often employed to approximate the nonlinear term shown in (2).

To improve the prediction accuracy, it is natural to carry out the calculation in a domain involving more mesh points. The resulting Navier–Stokes solutions become, however, more expensive and difficult to be computed because of the increasingly notorious eigenvalue distribution. For convergence acceleration without accuracy deterioration, the two-level method, which involves calculations carried out at the coarse mesh level and the other performed at the finer mesh level, has been proposed. For example, the solutions for (2) are obtained from a set of comparatively conditioned matrix equations on the coarse mesh. This is followed by solving the linearized Navier–Stokes equations only once on the fine mesh.

Various two-level methods have been proposed and were successfully applied to solve different classes of differential equations [8,13–15]. Of the proposed linearization methods for solving the Navier–Stokes equations, the Newton's method implemented either on the fixed mesh [16] or on the two successive meshes [17] has been often referred to. At a higher Reynolds number, implementation of Newton linearization may result

in a highly asymmetric and indefinite matrix. Both matrix asymmetry and indefiniteness are known to be the primary sources of yielding numerical instability. The matrix asymmetry arises from the approximation of convective terms while the matrix indefiniteness is attributed to the reaction term [12].

As a proper means to resolve the problem of indefiniteness, Layton and Lenferink [8] neglected the reaction term shown in the Newton linearized equation. The resulting Oseen linearized system of equations becomes computationally more easy to be solved and has been applied extensively in the past to analyze the Navier–Stokes equations [18]. Since the computational efficiency of the two-level Navier–Stokes methods depends strongly on the chosen linearization method, in the fine mesh the Oseen linearization [8] will be employed in this study. More recently, an additional defect correction step has been implemented in the coarse mesh to improve the prediction accuracy. One typical method of which is the modified Picard method used along with the correction step [18], which has been proven to be able to accelerate convergence.

The procedures of implementing the two-level Oseen-type Navier–Stokes method are as follows. The nonlinear system of equations for $(\mathbf{u}_H, p_H)$ is analyzed firstly on a coarse mesh of width H until the specified convergent condition is reached. This is followed by mapping the computed coarse mesh solutions to each point in the fine mesh with the grid size of h. After mapping the computed solutions, the pressure equation is solved using the prolongation velocity. The fine mesh solution $(\mathbf{u}_h, p_h)$ given below is then calculated from the linearized momentum equations and the pressure equation (3)

$$(\mathbf{u}_H \cdot \nabla)\mathbf{u}_h = -\nabla p_h + \frac{1}{Re}\nabla^2 \mathbf{u}_h + \mathbf{f}. \tag{6}$$

In the implementation of two-level methods, the bridge between the calculations performed at two grid levels is the prolongation matrix. Upon defining the prolongation operator, we are led to approximate the velocity vector $\mathbf{u}^*$ shown in the convective term $(\mathbf{u}^* \cdot \nabla)\mathbf{u}$ on the fine mesh. Note that the solution for $\mathbf{u}^*$ obtained from the coarse mesh should satisfy the full Navier–Stokes equations. An additional note is that the linearized momentum equations need to be solved only once to obtain $(\mathbf{u}_h, p_h)$ in the fine mesh. As a result, the computational quality of the employed two-level method depends solely on the value of $\mathbf{u}_H$, shown in (6), computed at the nodes marked by "○" and schematic in Fig. 1 in the fine mesh. This motivated us to develop a theoretical mapping strategy so as to accurately prolongate the computed convergent coarse mesh solutions to those at the fine mesh points.

To develop an effective prolongation operator, the following constant-coefficient equation is considered:

$$A\phi_x + B\phi_y = K\nabla^2\phi. \tag{7}$$

This equation is amenable to the exact solution given by

$$\phi(x,y) = \overline{A_1}e^{(\frac{Ax}{K})}e^{(\frac{By}{K})} + \overline{A_2}e^{(\frac{Ax}{K})} + \overline{A_3}e^{(\frac{By}{K})} + \overline{A_4}. \tag{8}$$

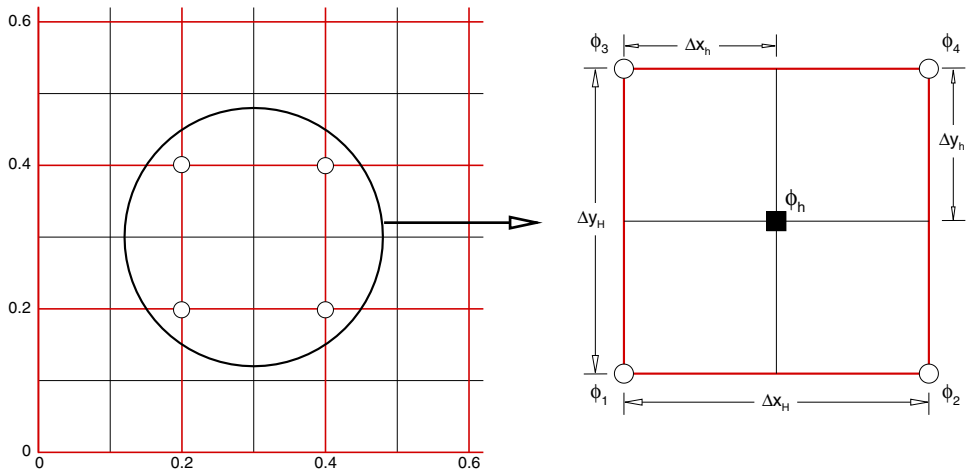

Fig. 1. A representative cell for the fine mesh (■) and coarse mesh (○).

Substitute the coordinates at the four points schematic in Fig. 1 into (8), the coefficients $\overline{A_1} \sim \overline{A_4}$ detailed in the Appendix can be derived in terms of the coarse mesh solutions $\phi_1 \sim \phi_4$. The values of ϕ at the rest of five nodal points can then be determined by means of (8).

4. Discretization of equation in non-staggered grids

4.1. Five-point convection–diffusion–reaction (CDR) scheme

The original idea of the analytical CDR scheme presented in [2] will be extended to the analysis of two-dimensional equation. In view of Eqs. (4) or (5), the following model equation for ϕ is considered for the sake of description of the CDR scheme:

$$a\phi_x + b\phi_y - k\nabla^2\phi + c\phi = f. \tag{9}$$

To eliminate the convective instability problem and to retain the prediction accuracy, the following general solution of the above model equation is employed:

$$\phi(x,y) = A_1 e^{\lambda_1 x} + A_2 e^{\lambda_2 x} + A_3 e^{\lambda_3 y} + A_4 e^{\lambda_4 y} + \frac{f}{c}, \tag{10}$$

where $\lambda_{1,2} = \frac{a \pm \sqrt{a^2+4ck}}{2k}$ and $\lambda_{3,4} = \frac{b \pm \sqrt{b^2+4ck}}{2k}$. The discrete equation at one interior node (i,j) is assumed to take the following five-point stencil form:

$$\begin{aligned}&\left(-\frac{a}{2h} - \frac{m}{h^2} + \frac{c}{12}\right)\phi_{i-1,j} + \left(\frac{a}{2h} - \frac{m}{h^2} + \frac{c}{12}\right)\phi_{i+1,j} + 4\left(\frac{m}{h^2} + \frac{2c}{12}\right)\phi_{i,j} \\ &+ \left(-\frac{b}{2h} - \frac{m}{h^2} + \frac{c}{12}\right)\phi_{i,j-1} + \left(\frac{b}{2h} - \frac{m}{h^2} + \frac{c}{12}\right)\phi_{i,j+1} = f_{i,j}.\end{aligned} \tag{11}$$

By substituting the exact solutions given by $\phi_{i,j} = A_1 e^{\lambda_1 x_i} + A_2 e^{\lambda_2 x_i} + A_3 e^{\lambda_3 y_j} + A_4 e^{\lambda_4 y_j} + \frac{f}{c}$, $\phi_{i\pm1,j} = A_1 e^{\pm\lambda_1 h} e^{\lambda_1 x_i} + A_2 e^{\pm\lambda_2 h} e^{\lambda_2 x_i} + A_3 e^{\lambda_3 y_j} + A_4 e^{\lambda_4 y_j} + \frac{f}{c}$ and $\phi_{i,j\pm1} = A_1 e^{\lambda_1 x_i} + A_2 e^{\lambda_2 x_i} + A_3 e^{\pm\lambda_3 h} e^{\lambda_3 y_j} + A_4 e^{\pm\lambda_4 h} e^{\lambda_4 y_j} + \frac{f}{c}$ into Eq. (11), m shown above can be derived as

$$\begin{aligned}m = &\left[\frac{ah}{2}\sinh\overline{\lambda_1}\cosh\overline{\lambda_2} + \frac{bh}{2}\sinh\overline{\lambda_3}\cosh\overline{\lambda_4} + \frac{ch^2}{12}(\cosh\overline{\lambda_1}\cosh\overline{\lambda_2} + \cosh\overline{\lambda_3}\cosh\overline{\lambda_4} + 10)\right] \Big/ \\ &(\cosh\overline{\lambda_1}\cosh\overline{\lambda_2} + \cosh\overline{\lambda_3}\cosh\overline{\lambda_4} - 2),\end{aligned} \tag{12}$$

where $(\overline{\lambda_1}, \overline{\lambda_2}) = \left(\frac{ah}{2k}, \sqrt{\left(\frac{ah}{2k}\right)^2 + \frac{ch^2}{k}}\right)$ and $(\overline{\lambda_3}, \overline{\lambda_4}) = \left(\frac{bh}{2k}, \sqrt{\left(\frac{bh}{2k}\right)^2 + \frac{ch^2}{k}}\right)$.

4.2. Approximation of ∇p

We will propose in this study two theoretically relevant schemes to discretize the pressure gradient term shown in Eq. (2) with an aim to avoid spurious pressure oscillations and prevent accuracy deterioration in the non-staggered mesh.

4.2.1. Dispersion-relation-preserving implicit pressure gradient scheme

The strategy of eliminating the even–odd solution profile is to take the nodal value of $p_{i,j}$ into account to calculate the approximated value of $\frac{\partial p}{\partial x}|_{i,j}$, for example, from the following implicit compact equation for $F_{i,j}(= h\frac{\partial p}{\partial x}|_{i,j})$ [19]:

$$\beta F_{i+1,j} + F_{i,j} + \gamma F_{i-1,j} = c_1 p_{i+2,j} + c_2 p_{i+1,j} + c_3 p_{i,j} + c_4 p_{i-1,j} + c_5 p_{i-2,j}. \tag{13}$$

In the above, h denotes the mesh size. On physical grounds, it is legitimate to set $\beta = \gamma$ since the governing equation for p is of the elliptic type. This is followed by carrying out the Taylor series expansions for $p_{i\pm1,j}$, $p_{i\pm2,j}$ with respect to $p_{i,j}$ and, then, eliminating the leading five error terms p, $\frac{\partial p}{\partial x}$, $\frac{\partial^2 p}{\partial x^2}$, $\frac{\partial^3 p}{\partial x^3}$, $\frac{\partial^4 p}{\partial x^4}$ from the resulting

modified equation to derive a system of five algebraic equations. One more algebraic equation needs to be derived so as to be able to uniquely determine the coefficients $\beta(=\gamma)$, c_1, c_2, c_3, c_4 and c_5 shown in (13).

When approximating the first-order derivative term, it is vital to preserve its dispersion-relation so that the resulting approximation can accommodate the same dispersion-relation as that of the first-order derivative term under discretization [20]. This dispersion-relation, which is derived by performing the spatial Fourier transform of the first derivative term, governs the relationship between the angular frequency and the wavenumber of the spatial variable [21]. The dispersiveness, dissipation, group and phase velocity components for each wave component supported by the first-order derivative term can be, therefore, well modeled [22]. Any scheme destabilization arising from the approximation of the first-order derivative term can be effectively suppressed [23].

Within the DRP (dispersion-relation-preserving) compact analysis framework [20,24], the Fourier transform and its inverse for $\frac{\partial p}{\partial x}$ are defined firstly in the one space dimension x as follows:

$$\tilde{p}(\alpha) = \frac{1}{2\pi}\int_{-\infty}^{+\infty} p(x)\mathrm{e}^{-\mathbf{i}\alpha x}\,\mathrm{d}x, \tag{14}$$

$$p(x) = \int_{-\infty}^{+\infty} \tilde{p}(\alpha)\mathrm{e}^{\mathbf{i}\alpha x}\,\mathrm{d}\alpha. \tag{15}$$

By conducting Fourier transform on each term shown in Eq. (13), we are led to derive the following actual wavenumber α:

$$\alpha \simeq \frac{-\mathbf{i}}{h}\frac{(c_1\,\mathrm{e}^{\mathbf{i}2\alpha h} + c_2\,\mathrm{e}^{\mathbf{i}\alpha h} + c_3 + c_4\,\mathrm{e}^{-\mathbf{i}\alpha h} + c_5\,\mathrm{e}^{-\mathbf{i}2\alpha h})}{1+\beta(\mathrm{e}^{\mathbf{i}\alpha h}+\mathrm{e}^{-\mathbf{i}\alpha h})}. \tag{16}$$

In the approximation sense, the effective wavenumber $\tilde{\alpha}$ can be regarded as the right-hand side of Eq. (16) [20]. In other words, we are led to define $\tilde{\alpha}$ as follows:

$$\tilde{\alpha} = \frac{-\mathbf{i}}{h}\frac{(c_1\,\mathrm{e}^{\mathbf{i}2\alpha h} + c_2\,\mathrm{e}^{\mathbf{i}\alpha h} + c_3 + c_4\,\mathrm{e}^{-\mathbf{i}\alpha h} + c_5\,\mathrm{e}^{-\mathbf{i}2\alpha h})}{1+\beta(\mathrm{e}^{\mathbf{i}\alpha h}+\mathrm{e}^{-\mathbf{i}\alpha h})}, \tag{17}$$

where $\mathbf{i} = \sqrt{-1}$. To make α be close to $\tilde{\alpha}$, the magnitude of $|\alpha h - \tilde{\alpha}h|^2$ should be kept as small as possible in the following weak sense:

$$E(\alpha) = \int_{-\frac{\pi}{2}}^{\frac{\pi}{2}} W|\alpha h - \tilde{\alpha}h|^2\mathrm{d}(\alpha h) = \int_{-\frac{\pi}{2}}^{\frac{\pi}{2}} W|\mathbf{i}\gamma - \tilde{\gamma}|^2\mathrm{d}\gamma, \tag{18}$$

where $\gamma = \alpha h$. Note that Eq. (18) can be analytically integrable provided that the weighting function W shown above is chosen as [25,26]

$$W = [1+\beta(\mathrm{e}^{\mathbf{i}\gamma}+\mathrm{e}^{-\mathbf{i}\gamma})]^2. \tag{19}$$

In Eq. (18), the modified wavenumber range should be sufficient to define a period of sine (or cosine) wave. This explains why the integral range has been chosen to be $-\frac{\pi}{2} \le \gamma \le \frac{\pi}{2}$ [27]. To make E a minimum positive value, the following equation is enforced to achieve the goal:

$$\frac{\partial E}{\partial c_2} = 0. \tag{20}$$

According to the above extreme condition, we are led to derive one algebraic equation, which will be used together with the other five equations derived from the modified equation analysis. Having derived the sufficient number of algebraic equations, the six introduced coefficients given below can be derived:

$$\beta = \gamma = \frac{4(3\pi-10)}{3\pi-16}, \tag{21}$$

$$c_1 = \frac{3(5\pi-16)}{4(3\pi-16)}, \tag{22}$$

$$c_2 = \frac{6(\pi-4)}{3\pi-16}, \tag{23}$$

$$c_3 = 0, \tag{24}$$

$$c_4 = -\frac{6(\pi-4)}{3\pi-16}, \tag{25}$$

$$c_5 = -\frac{3(5\pi-16)}{4(3\pi-16)}. \tag{26}$$

The resulting modified equation for $\frac{\partial p}{\partial x}$ can be easily shown to have the spatial accuracy order of fourth:

$$\frac{\partial p}{\partial x} = \left.\frac{\partial p}{\partial x}\right|_{\text{exact}} + \frac{(33\pi-104)}{30(3\pi-16)} h^4 \frac{\partial^5 p}{\partial x^5} + \mathrm{O}(h^6) + \cdots \tag{27}$$

Note that enforcement of $\frac{\partial E}{\partial c_4} = 0$ can also lead to the same result as that given in Eq. (20). To obtain the discrete equations for $F_{i,j}(\equiv h\frac{\partial p}{\partial x}|_{i,j})$ at the nodes immediately adjacent to the boundary points, it is legitimate to specify $c_1 = 0$ and $c_5 = 0$ for the nodes located next to the left and right boundaries, respectively.

4.2.2. Dispersion-relation-preserving explicit pressure gradient scheme

Inversion of the matrix equation given by (13) can be computationally very costly for the implicit compact scheme (with the coefficients given by (21)–(26)) when the matrix size is large. We are therefore motivated to reformulate the compact scheme by proposing an explicit pressure gradient scheme. It is required that the property of implicit compact scheme given in Section 4.2.1 be still retained. Calculation of the value for ∇p in non-staggered grids can, thus, be accelerated without accuracy deterioration.

In the seven-point solution stencil schematic in Fig. 2, the implicit equation for $\frac{\partial p}{\partial x}$ can be expressed in the matrix form given below for the vector $\underline{\mathbf{P}}(\equiv (p_1, p_2, \ldots, p_7)^{\mathrm{T}})$:

$$\underline{\underline{\mathbf{A}}}\,\underline{\mathbf{P}}_{\mathbf{x}} = \underline{\underline{\mathbf{B}}}\,\underline{\mathbf{P}}, \tag{28}$$

where

$$\underline{\underline{\mathbf{A}}} = \begin{bmatrix}
1 & \frac{4}{-8+3\pi} & & & & & \\
\frac{2(3\pi-10)}{-224+69\pi} & 1 & \frac{51\pi-164}{-224+69\pi} & & & & \\
 & \frac{4(3\pi-10)}{3\pi-16} & 1 & \frac{4(3\pi-10)}{3\pi-16} & & & \\
 & & \frac{4(3\pi-10)}{3\pi-16} & 1 & \frac{4(3\pi-10)}{3\pi-16} & & \\
 & & & \frac{4(3\pi-10)}{3\pi-16} & 1 & \frac{4(3\pi-10)}{3\pi-16} & \\
 & & & & \frac{51\pi-164}{-224+69\pi} & 1 & \frac{2(3\pi-10)}{-224+69\pi} \\
 & & & & & \frac{4}{-8+3\pi} & 1
\end{bmatrix},$$

$$\underline{\underline{\mathbf{B}}} = \begin{bmatrix}
-\frac{33\pi-80}{6(-8+3\pi)} & \frac{9\pi-26}{-8+3\pi} & -\frac{9\pi-32}{2(-8+3\pi)} & \frac{3\pi-10}{3(-8+3\pi)} & & & \\
-\frac{3(17\pi-56)}{2(-224+69\pi)} & -\frac{27(5\pi-16)}{2(-224+69\pi)} & \frac{3(57\pi-184)}{2(-224+69\pi)} & \frac{3(5\pi-16)}{2(-224+69\pi)} & & & \\
-\frac{6(\pi-4)}{3\pi-16} & -\frac{6(\pi-4)}{3\pi-16} & 0 & \frac{6(\pi-4)}{3\pi-16} & \frac{3(5\pi-16)}{4(3\pi-16)} & & \\
 & -\frac{6(\pi-4)}{3\pi-16} & -\frac{6(\pi-4)}{3\pi-16} & 0 & \frac{6(\pi-4)}{3\pi-16} & \frac{3(5\pi-16)}{4(3\pi-16)} & \\
 & & -\frac{6(\pi-4)}{3\pi-16} & -\frac{6(\pi-4)}{3\pi-16} & 0 & \frac{6(\pi-4)}{3\pi-16} & \frac{3(5\pi-16)}{4(3\pi-16)} \\
 & & & -\frac{3(5\pi-16)}{2(-224+69\pi)} & -\frac{3(57\pi-184)}{2(-224+69\pi)} & \frac{27(5\pi-16)}{2(-224+69\pi)} & \frac{3(17\pi-56)}{2(-224+69\pi)} \\
 & & & -\frac{3\pi-10}{3(-8+3\pi)} & \frac{9\pi-32}{2(-8+3\pi)} & -\frac{9\pi-26}{-8+3\pi} & \frac{33\pi-80}{6(-8+3\pi)}
\end{bmatrix}.$$

The pressure gradient vector $\underline{\mathbf{P}}_{\mathbf{x}}$ $(\equiv (\frac{\partial p}{\partial x}|_1, \frac{\partial p}{\partial x}|_2, \ldots, \frac{\partial p}{\partial x}|_7)^{\mathrm{T}})$ in Eq. (28) can be also written as $\underline{\mathbf{P}}_{\mathbf{x}} = \underline{\underline{\mathbf{G}}}\,\underline{\mathbf{P}}$, where $\underline{\underline{\mathbf{G}}}$ $(\equiv \underline{\underline{\mathbf{A}}}^{-1}\underline{\underline{\mathbf{B}}})$ is expressed as

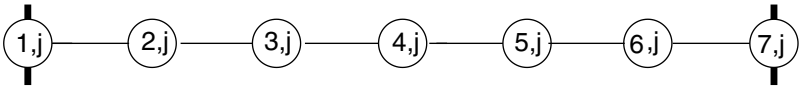

Fig. 2. Nodal numbering of the interior points 2–6 and the boundary points 1 and 7.

$$\underline{\underline{\mathbf{G}}} = \begin{bmatrix} -2.131201 & 4.306948 & -3.781477 & 2.346956 & -0.953555 & 0.244597 & -0.032269 \\ -0.227239 & -0.965525 & 1.812651 & -0.883908 & 0.339651 & -0.087124 & 0.011494 \\ 0.054353 & -0.507185 & -0.360289 & 1.092619 & -0.359561 & 0.092231 & -0.012167 \\ -0.023277 & 0.176444 & -0.783056 & 0 & 0.783056 & -0.176444 & 0.023277 \\ 0.012167 & -0.092231 & 0.359561 & -1.092619 & 0.360289 & 0.507185 & -0.054353 \\ -0.011494 & 0.087124 & -0.339651 & 0.883908 & -1.812651 & 0.965525 & 0.227239 \\ 0.032269 & -0.244597 & 0.953555 & -2.346956 & 3.781477 & -4.306948 & 2.131201 \end{bmatrix}. \tag{29}$$

In $\underline{\underline{\mathbf{G}}}$, it is found that the sum of the columns from 2 to $n-1$ is zero. The skew-symmetry matrix $\underline{\underline{\mathbf{G}}}$ can, therefore, be classified as the global conservation type [28]. In view of the resulting modified equations given below, the compact approximation of $\frac{\partial p}{\partial x}$, for example, at the three nodes schematic in Fig. 2 introduces different amounts of the implicit dissipation error to the analytic pressure gradient solution:

$$\frac{\partial p}{\partial x} = \left.\frac{\partial p}{\partial x}\right|_{\text{exact}} + 0.035382h^3\frac{\partial^4 p}{\partial x^4} - 0.078237h^4\frac{\partial^5 p}{\partial x^5} + \mathrm{O}(h^5) + \cdots; \quad \text{at node 1,} \tag{30}$$

$$\frac{\partial p}{\partial x} = \left.\frac{\partial p}{\partial x}\right|_{\text{exact}} - 0.006890h^3\frac{\partial^4 p}{\partial x^4} + 0.024948h^4\frac{\partial^5 p}{\partial x^5} + \mathrm{O}(h^5) + \cdots; \quad \text{at node 2,} \tag{31}$$

$$\frac{\partial p}{\partial x} = \left.\frac{\partial p}{\partial x}\right|_{\text{exact}} + 0.002419h^3\frac{\partial^4 p}{\partial x^4} - 0.014102h^4\frac{\partial^5 p}{\partial x^5} + \mathrm{O}(h^5) + \cdots; \quad \text{at node 3.} \tag{32}$$

We now proceed to refine the above implicit scheme by constructing an explicit pressure gradient scheme so that the essence of the DRP implicit compact scheme described in Section 4.2.1 can be retained. Examination of Eq. (29) reveals that the proposed compact scheme given in Eqs. (28) and (29) has the following two properties for a $N \times N$ matrix $\underline{\underline{\mathbf{G}}}$:

(a) $\underline{\underline{\mathbf{G}}}(m, n-1) \times \underline{\underline{\mathbf{G}}}(m+1, n) = \underline{\underline{\mathbf{G}}}(m, n) \times \underline{\underline{\mathbf{G}}}(m+1, n-1)$, where $m = 1 \sim N/2 - 1$, $n = 6 \sim N$;
(b) $\underline{\underline{\mathbf{G}}}(m, 1:N) = -\underline{\underline{\mathbf{G}}}(N-m+1, N:1)$, $m = 1 \sim N/2$.

Referring to Fig. 3(a), at an interior point (i, j) in the mesh with the grid size of h, $p_x|_{i,j}$ is approximated by the following equation:

$$\left.\frac{\partial p}{\partial x}\right|_{i,j} = a_1 p_{i+3,j} + a_2 p_{i+2,j} + a_3 p_{i+1,j} - a_3 p_{i-1,j} - a_2 p_{i-2,j} - a_1 p_{i-3,j}. \tag{33}$$

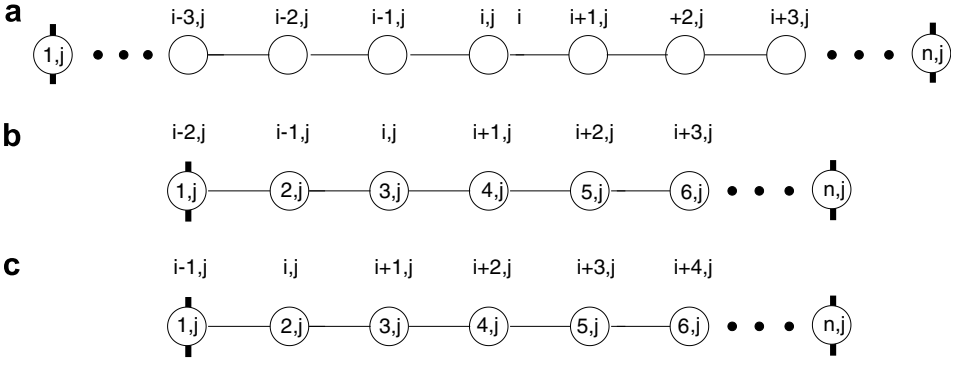

Fig. 3. Nodal numbering of the interior points in (a) and the boundary points in (b) and (c).

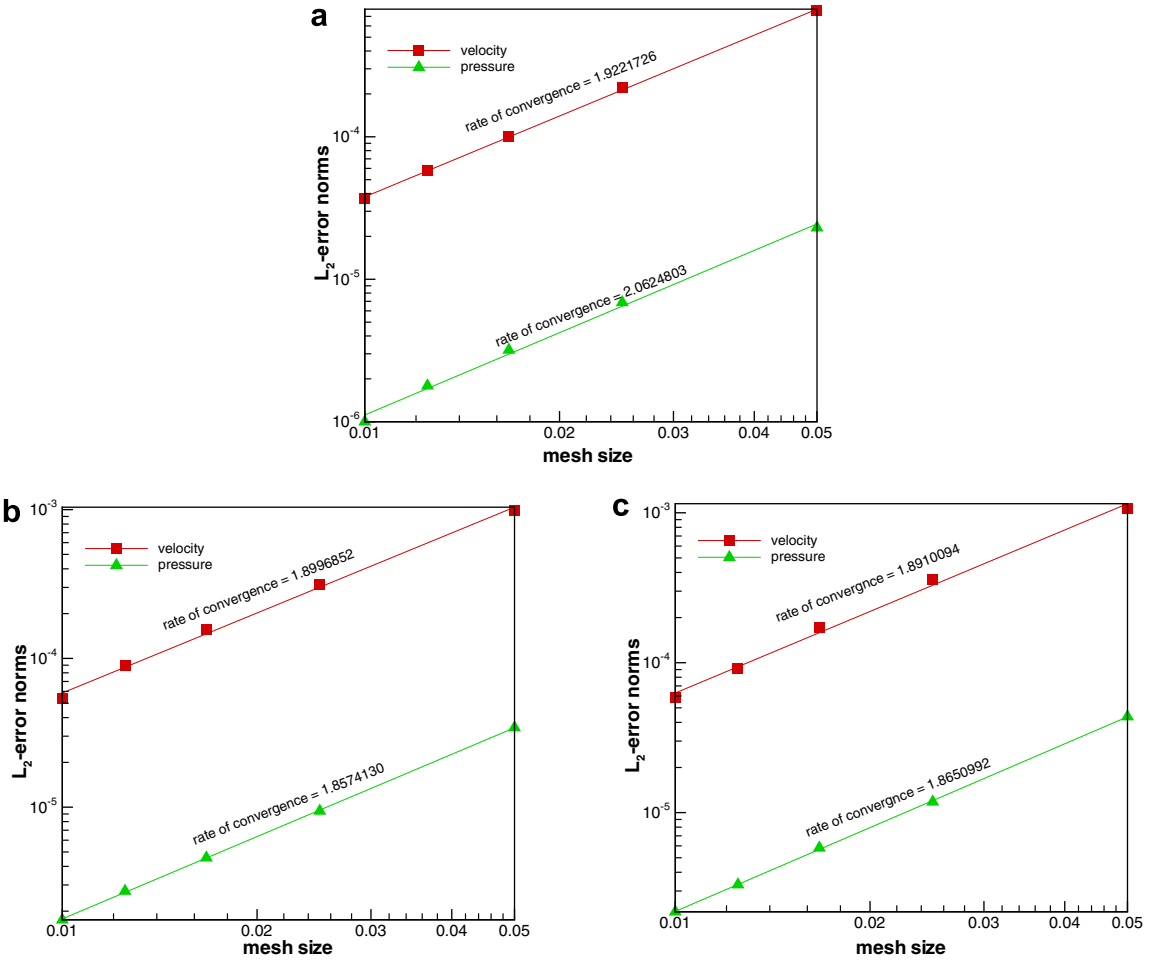

Fig. 4. The computed spatial rates of convergence for velocity and pressure using the proposed Oseen-type two-level method and the one-level method. (a) Direct (one-level) method; (b) Oseen implicit method; (c) Oseen explicit method.

Table 1
Comparison of the predicted L_2-error norms for the calculations carried out at five chosen mesh sizes using the employed different methods

Mesh points	Velocity **u**			Pressure p		
	Direct	Oseen (implicit)	Oseen (explicit)	Direct	Oseen (implicit)	Oseen (explicit)
21×21	7.65E−04	9.88E−04	1.07E−03	2.30E−05	3.43E−05	4.37E−05
41×41	2.22E−04	3.14E−04	3.59E−04	6.88E−06	9.43E−06	1.18E−05
61×61	1.01E−04	1.57E−04	1.72E−04	3.19E−06	4.57E−06	5.82E−06
81×81	5.79E−05	8.93E−05	9.12E−05	1.79E−06	2.73E−06	3.31E−06
101×101	3.68E−05	5.37E−05	5.87E−05	1.00E−06	1.75E−06	2.18E−06

This is followed by applying the Taylor series expansions for $p_{i\pm1,j}$, $p_{i\pm2,j}$ and $p_{i\pm3,j}$ with respect to $p_{i,j}$ and, then, eliminating the leading error terms $\frac{\partial p}{\partial x}$ and $\frac{\partial^3 p}{\partial x^3}$ shown in the resulting modified equation. One more algebraic equation needs to be derived for uniquely determining the coefficients a_1, a_2 and a_3 shown in (33). By conducting the same Fourier transform and the minimization of dispersion error as those described in Section 4.2.1, the following coefficients a_i $(i = 1\text{–}3)$ can be derived:

Table 2
Comparison of the required CPU times (s) at the same accuracy level and the needed numbers of iterations N and N_c, where N and N_c are the iteration numbers performed on the respective fine mesh (one-level method) and coarse mesh (two-level method) when solving the nonlinear momentum equations using the employed three methods at five different mesh sizes

Direct			Oseen (implicit)		
Mesh points	CPU-time (L_2-error)	N	Mesh points	CPU-time (L_2-error)	N_c
21×21	10.71 (7.65E−04)	158	25×25	2.84 (7.32E−04)	19
41×41	28.87 (2.22E−04)	201	51×51	8.87 (2.13E−04)	68
61×61	60.45 (1.01E−04)	475	81×81	20.46 (8.93E−05)	219
81×81	151.27 (5.79E−05)	1291	101×101	38.95 (5.37E−05)	335
101×101	353.56 (3.68E−05)	1965	121×121	75.54 (3.87E−05)	524
21×21	10.71 (7.65E−04)	158	25×25	2.42 (7.88E−04)	19
41×41	28.87 (2.22E−04)	201	51×51	6.53 (2.35E−04)	69
61×61	60.45 (1.01E−04)	475	81×81	14.69 (9.12E−05)	216
81×81	151.27 (5.79E−05)	1291	101×101	29.53 (5.87E−05)	331
101×101	353.56 (3.68E−05)	1965	121×121	60.32 (4.23E−05)	528

Note that the values "·" in $(\cdot)$ represent the computed L_2-error norms.

$$a_1 = -\frac{2(-10+3\pi)}{3(-32+15\pi)}, \tag{34}$$

$$a_2 = \frac{3(-32+9\pi)}{4(-32+15\pi)}, \tag{35}$$

$$a_3 = \frac{12}{-32+15\pi}. \tag{36}$$

The corresponding modified equation for the explicit approximation of $\frac{\partial p}{\partial x}$ can be derived as

$$\frac{\partial p}{\partial x} = \frac{\partial p}{\partial x}|_{\text{exact}} - \frac{9(5\pi-16)}{10(-32+15\pi)} h^4 \frac{\partial^5 p}{\partial x^5} + O(h^6) + \cdots. \tag{37}$$

For the points near the boundary, some modifications need to be made for $(i = 2, j)$ and $(i = 3, j)$ schematic in Fig. 3(b) and (c) so as to retain property (a):

(i) For $i = 3, j$
Referring to Fig. 3(b), we can approximate $\frac{\partial p}{\partial x}$ at node 3 in terms of the nodal pressure values $p_{i,j}, p_{i\pm2,j}, p_{i+3,j}$ as

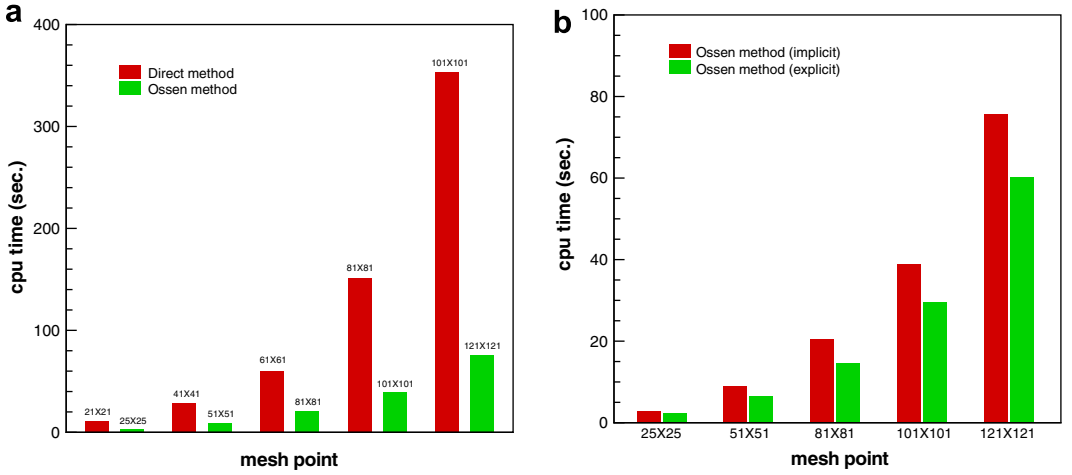

Fig. 5. Comparison of the CPU times (s) needed for the proposed two-level method and the one-level method at the same accuracy level for analyses carried out at different mesh sizes. (a) Direct (one-level) and Oseen (two-level) methods; (b) Oseen implicit and Oseen explicit methods.

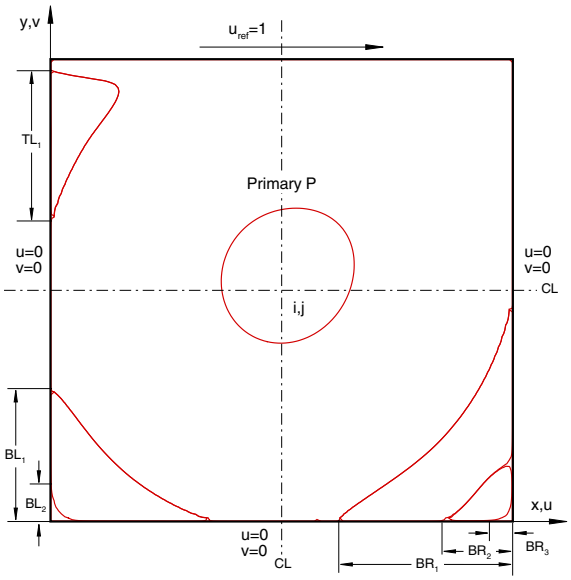

Fig. 6. Schematic of the predicted eddy centers in the lid-driven cavity.

Table 3
The predicted four eddy centers (primary eddy P, corner eddies BL and BR and the eddy T near the cavity roof) for the cases carried out at $Re = 400$, 1000, 3200 and 5000

Symbol	Authors	*Re*			
		400	1000	3200	5000
Primary	Present	0.5579, 0.6112	0.5331, 0.5745	0.5235, 0.5357	0.5207, 0.5305
	Ghia [29]	0.5547, 0.6055	0.5313, 0.5625	0.5165, 0.5469	0.5117, 0.5352
	Erturk [30]	–	0.5300, 0.5650	–	0.5150, 0.5350
First T	Present	–	–	0.0561, 0.8951	0.0622, 0.8986
	Ghia [29]	–	–	0.0547, 0.8984	0.0625, 0.9102
	Erturk [30]	–	–	–	0.0633, 0.9100
BL1	Present	0.0548, 0.0438	0.0821, 0.0754	0.0835, 0.1097	0.0747, 0.1272
	Ghia [29]	0.0508, 0.0469	0.0859, 0.0781	0.0859, 0.1094	0.0703, 0.1367
	Erturk [30]	–	0.0833, 0.0783	–	0.0733, 0.1367
BR1	Present	0.8807, 0.1261	0.8542, 0.1187	0.9051, 0.0650	0.8048, 0.0726
	Ghia [29]	0.8906, 0.1250	0.8594, 0.1094	0.8125, 0.0859	0.8086, 0.0742
	Erturk [30]	–	0.8633, 0.1117	–	0.8050, 0.0733
Second BL2	Present	0.0036, 0.0037	0.0046, 0.0043	0.0075, 0.0076	0.0107, 0.0076
	Ghia [29]	0.0039, 0.0039	–	0.0078, 0.0078	0.0117, 0.0078
	Erturk [30]	–	0.0050, 0.0050	–	0.0083, 0.0083
BR2	Present	0.9897, 0.0076	0.9897, 0.0076	0.9812, 0.0076	0.9795, 0.0189
	Ghia [29]	0.9922, 0.0078	0.9922, 0.0078	0.9844, 0.0078	0.9805, 0.0195
	Erturk [30]	–	0.9917, 0.0067	–	0.9783, 0.0183
Third BR3	Present	–	–	–	–
	Ghia [29]	–	–	–	–
	Erturk [30]	–	–	–	–
Grid size	Present	81	101	101	129
	Ghia [29]	129	129	129	257
	Erturk [30]	–	601	–	601

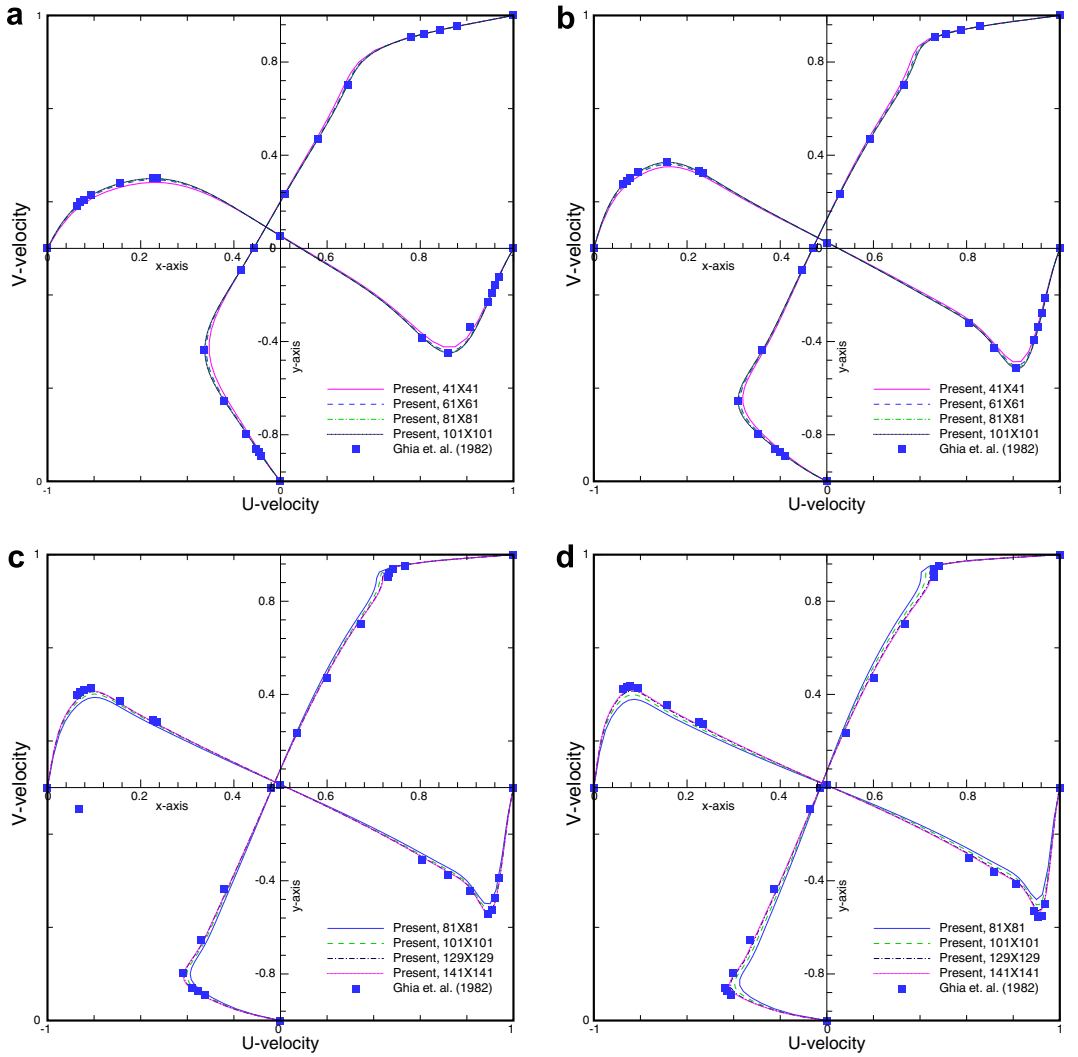

Fig. 7. Comparison of the predicted mid-plane velocity profiles for $u(x, 0.5)$ and $v(0.5, y)$. (a) $Re = 400$; (b) $Re = 1000$; (c) $Re = 3200$; (d) $Re = 5000$.

$$\left.\frac{\partial p}{\partial x}\right|_{i=3,j} = b_1 p_{i-2,j} + b_2 p_{i-1,j} + b_3 p_{i,j} + b_4 p_{i+1,j} + b_5 p_{i+2,j} + b_6 p_{i+3,j}. \tag{38}$$

By eliminating the leading error terms to $\frac{\partial^4 p}{\partial x^4}$ and enforcing the coefficient of $\frac{\partial^5 p}{\partial x^5}$ to be $-\frac{9(5\pi-16)}{10(-32+a5\pi)}$, we can derive $b_1 = \frac{-64+21\pi}{4(-32+15\pi)}$, $b_2 = \frac{2(-44+15\pi)}{-32+15\pi}$, $b_3 = \frac{40(3\pi-10)}{3(-32+15\pi)}$, $b_4 = \frac{2(-56+15\pi)}{-32+15\pi}$, $b_5 = \frac{-256+75\pi}{4(-32+15\pi)}$, $b_6 = \frac{4(3\pi-10)}{3(-32+15\pi)}$. The resulting modified equation, given by $\frac{\partial p}{\partial x} = \frac{\partial p}{\partial x}|_{\text{exact}} - \frac{9(5\pi-16)}{10(-32+15\pi)} h^4 \frac{\partial^5 p}{\partial x^5} - \frac{2(3\pi-10)}{3(-32+15\pi)} h^5 \frac{\partial^6 p}{\partial x^6} + O(h^6) + \cdots$, implies that the damping term has been implicitly introduced to the central-type DRP scheme.

(ii) For $i = 2, j$

Referring to Fig. 3(c) and taking property (a) into account, the approximated expression for $\frac{\partial p}{\partial x}$ at point 2 is assumed to take the following form:

$$\left.\frac{\partial p}{\partial x}\right|_{i=2,j} = d_1 p_{i-1,j} + d_2 p_{i,j} + d_3 p_{i+1,j} + d_4 p_{i+2,j} + d_5 p_{i+3,j} + d_6 p_{i+4,j}. \tag{39}$$

By enforcing property (a), we are led to express $\frac{\partial p}{\partial x}|_{j=2}$ given below

$$\left.\frac{\partial p}{\partial x}\right|_{j=2} = d_1 p_{j-1} + d_2 p_j + d_3 p_{j+1} + d_4 p_{j+2} + d_5 p_{j+3} + \left(\frac{c_6}{c_5} d_5\right) P_{j+4}, \tag{40}$$

where $\frac{c_6}{c_5} = -\frac{16(3\pi-10)}{3(-256+75\pi)}$. By eliminating the leading error terms prior to $\frac{\partial^5 p}{\partial x^5}$, the six introduced coefficients can be derived as $d_1 = -\frac{93\pi-256}{12(15\pi-32)}$, $d_2 = \frac{5(3\pi-16)}{15\pi-32}$, $d_3 = -\frac{105\pi-512}{6(15\pi-32)}$, $d_4 = \frac{195\pi-704}{6(15\pi-32)}$, $d_5 = \frac{-256+75\pi}{4(15\pi-32)}$, $d_6 = \frac{4(3\pi-10)}{3(15\pi-32)}$. The corresponding modified equation can be derived as $\frac{\partial p}{\partial x} = \frac{\partial p}{\partial x}|_{\text{exact}} + \frac{285\pi-896}{60(-32+15\pi)} h^4 \frac{\partial^5 p}{\partial x^5} + \frac{159\pi-512}{24(-32+15\pi)} h^5 \frac{\partial^6 p}{\partial x^6} + O(h^6) + \cdots$. The approximated equations for p_x near the boundary points $(i = n-2, j)$ and $(i = n-1, j)$ schematic in Fig. 3 can be similarly derived by taking property (b) into account. Based on the above formulation, the proposed explicit scheme for approximating the pressure gradient term has been shown to have the theoretical spatial accuracy order of fourth. Both the compact and DRP properties inherent in the implicit scheme for ∇p, discussed in Section 4.2.1, are retained using the proposed computationally less expensive explicit pressure gradient scheme.

5. Numerical results

5.1. Analytic Navier–Stokes problem

We will verify the proposed two-level Navier–Stokes solver by solving the problem, defined in $0 \leq x, y \leq 1$, amenable to the following exact solutions:

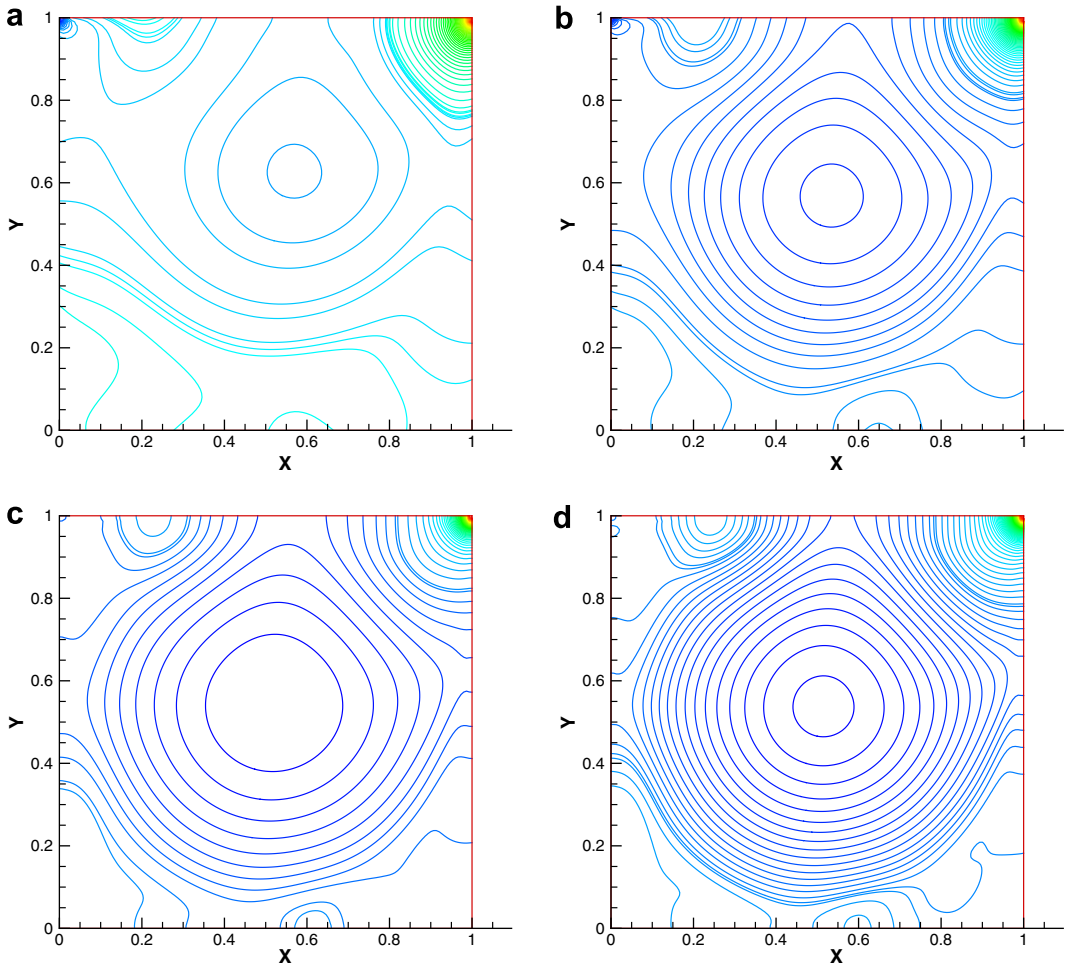

Fig. 8. The predicted pressure contours at different Reynolds numbers. (a) $Re = 400$; (b) $Re = 1000$; (c) $Re = 3200$; (d) $Re = 5000$.

$$u = \frac{-2(1+y)}{(1+x)^2 + (1+y)^2}, \tag{41}$$

$$v = \frac{2(1+x)}{(1+x)^2 + (1+y)^2}, \tag{42}$$

$$p = -\frac{2}{(1+x)^2 + (1+y)^2}. \tag{43}$$

We plot the values of $\log(\frac{err_1}{err_2})$ against $\log(\frac{h_1}{h_2})$, where the L_2 error norms err_1 and err_2 are obtained at two consecutively refined mesh sizes h_1 and h_2, to calculate the scheme's rate of convergence. In Fig. 4, the predicted quadratic spatial rates of convergence for **u** and p, computed from the respective L_2-error norms, are the consequence of applying the central scheme to the right-hand side of Eq. (3). In Table 1, the predicted solutions at $Re = 1000$ are in good agreement with the exact solutions. The proposed two-level method is, therefore, verified.

We also assess the one- and two-level methods in terms of the predicted L_2-error norms and the elapsed CPU time needed to reach the user's specified tolerance set for the nonlinear (or outer) iteration (10^{-12}) at

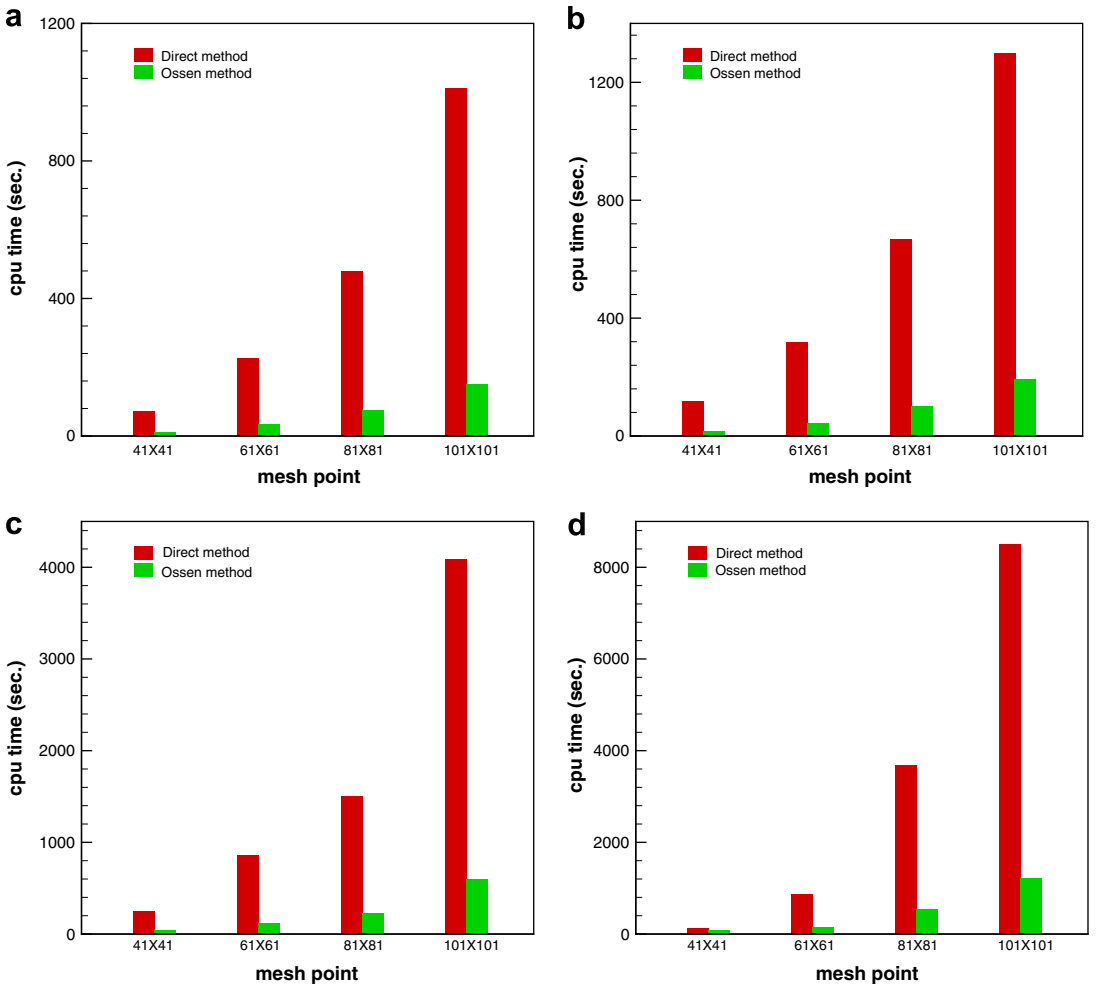

Fig. 9. Comparison of the needed CPU times (s) for the calculations carried out at different mesh points. (a) $Re = 400$; (b) $Re = 1000$; (c) $Re = 3200$; (d) $Re = 5000$.

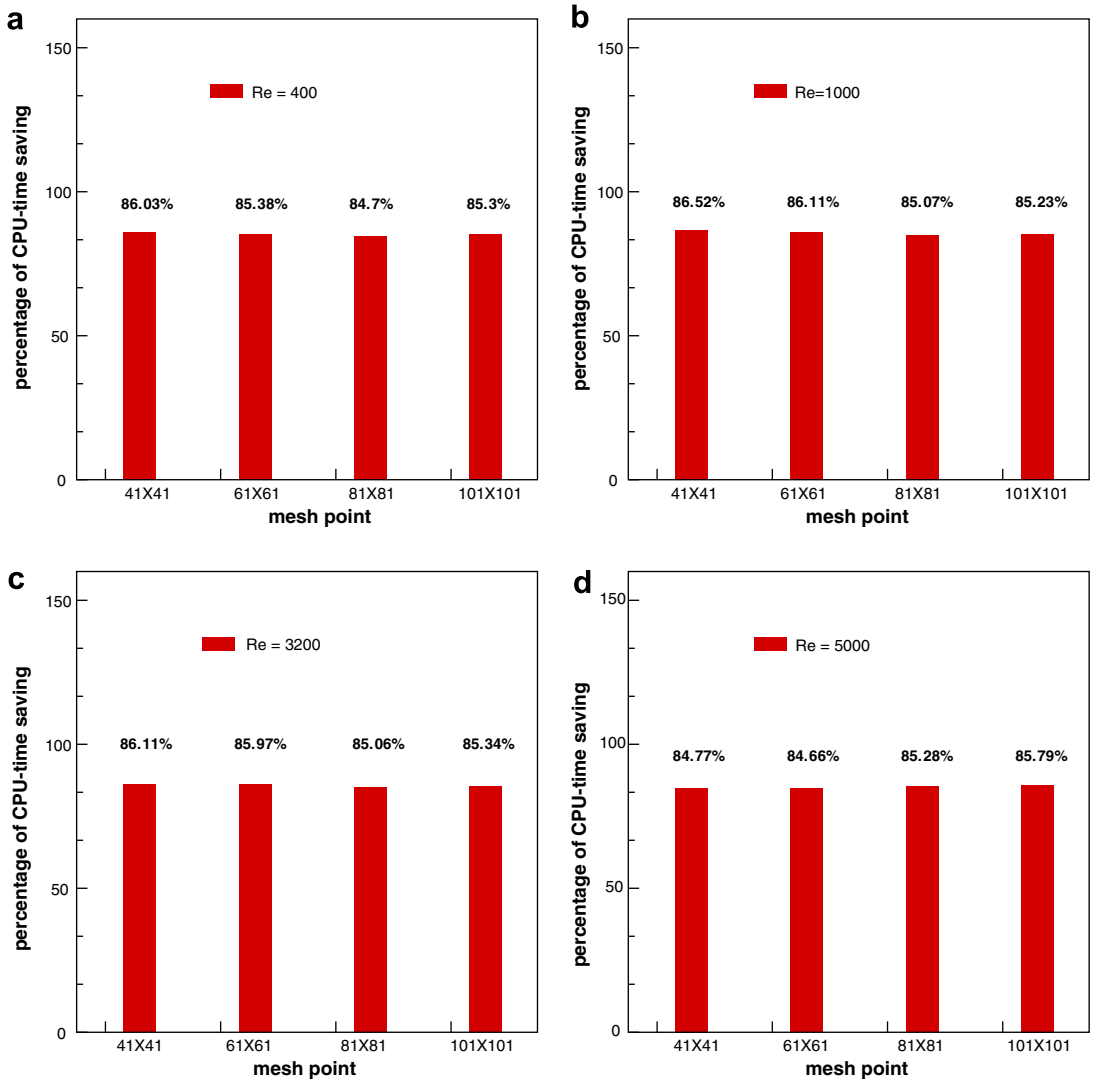

Fig. 10. Comparison of the reduced percentages of the CPU time for the calculations carried out at different mesh points. (a) $Re = 400$; (b) $Re = 1000$; (c) $Re = 3200$; (d) $Re = 5000$.

the same accuracy level and, of course, the needed nonlinear iteration numbers. As Table 1 tabulates, the predicted two-level Navier–Stokes solutions have been slightly deteriorated. Such a negligibly small deterioration in accuracy can save, however, a large amount of CPU time, as clearly demonstrated in Table 2 and in Fig. 5. The superiority of accelerating the Navier–Stokes calculation is clearly demonstrated using the proposed two-level method. In addition, the number of nonlinear iterations has been considerably reduced.

5.2. Lid-driven cavity flow problem

The flow driven by a constant upper lid velocity $u_{\text{lid}}(= 1)$ in the square cavity is then investigated at different Reynolds numbers. With $L(= 1)$ chosen as the characteristic length, $u_{\text{lid}}(= 1)$ the characteristic velocity, and v the fluid viscosity, the Reynolds numbers under investigation are $Re = 400$, 1000, 3200 and 5000. For the sake of completeness, the centers of the three predicted eddies T, BL and BR schematic in Fig. 6 are summarized in Table 3 for the cases investigated at $Re = 400$, 1000, 3200 and 5000. The predicted grid-independent mid-plane velocity profiles for $u(0.5, y)$ and $v(x, 0.5)$ are plotted in Fig. 7. Good agreement with the benchmark solutions

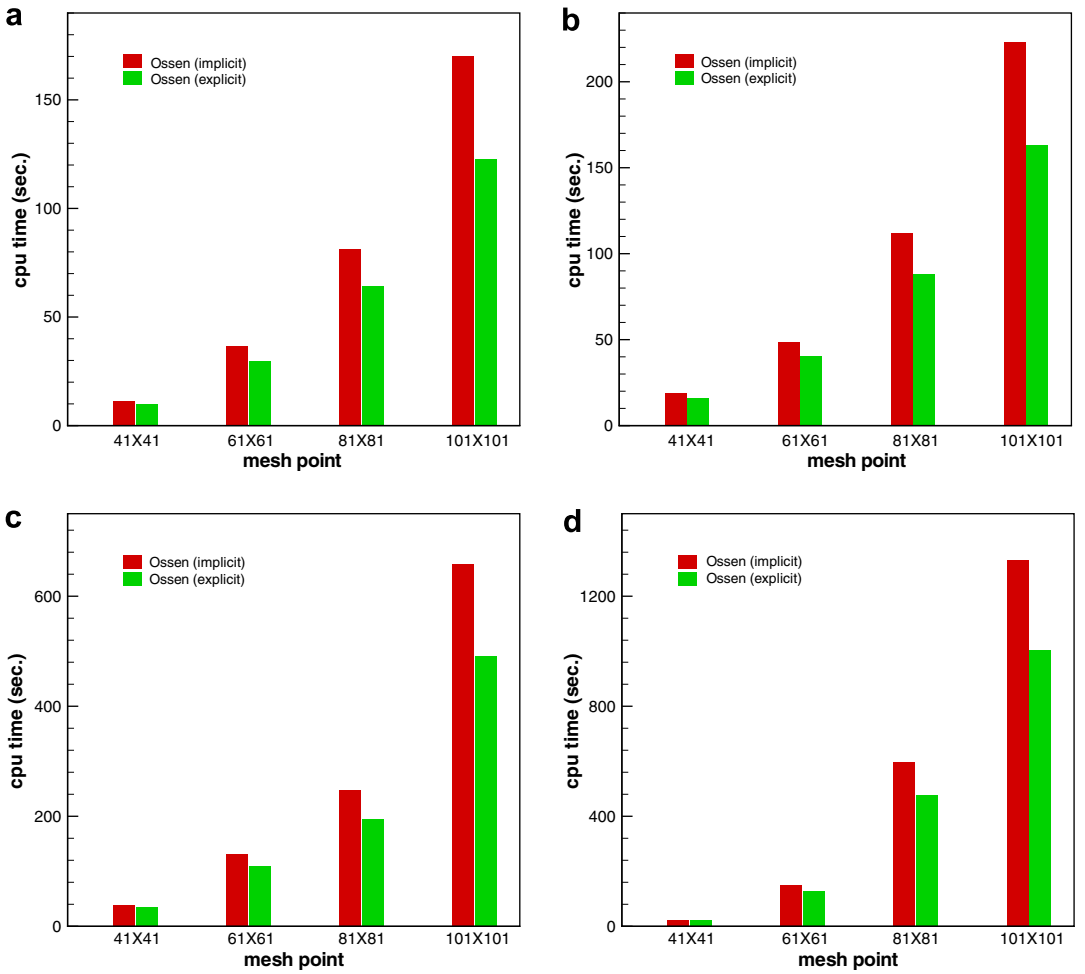

Fig. 11. Comparison of the two proposed schemes in CPU times (s) for approximating ∇p in the non-staggered grids of different mesh points. (a) $Re = 400$; (b) $Re = 1000$; (c) $Re = 3200$; (d) $Re = 5000$.

of Ghia [29] (■) and Erturk [30] (○) verifies the proposed scheme. To address that the proposed explicit scheme for approximating the pressure gradient term can suppress the even–odd pressure oscillations, we plot in Fig. 8 the pressure contours. It can be clearly seen from these figures that the pressure contours have been smoothly predicted at all investigated Reynolds numbers.

For demonstrating the efficiency of the employed two-level method, the required nonlinear iteration numbers for the case carried out at 128×128 mesh points and for the flow conditions investigated at $Re = 400$, 1000, 3200 and 5000 will be counted. Note that the nonlinear calculations for the two-level and one-level methods are performed at 128×128 and 256×256 mesh points, respectively. Since the number of nonlinear iterations can be considerably reduced for the calculation carried out in the fine mesh, much of the CPU time can, therefore, be reduced as well (Fig. 9). The higher the Reynolds number, the larger percentage of the CPU time can be saved (Fig. 10).

Within the Oseen two-level analysis framework, the effectiveness of applying the implicit and explicit DRP pressure gradient schemes is also assessed in terms of the needed CPU time. As can be seen from Fig. 11, one quarter of the CPU time can be saved using the proposed explicit pressure gradient scheme implemented in the non-staggered grids. Also, the saving of CPU time from the explicit pressure gradient scheme seems to be irrelevant to the Reynolds number, as can be clearly seen from Figs. 12 and 13.

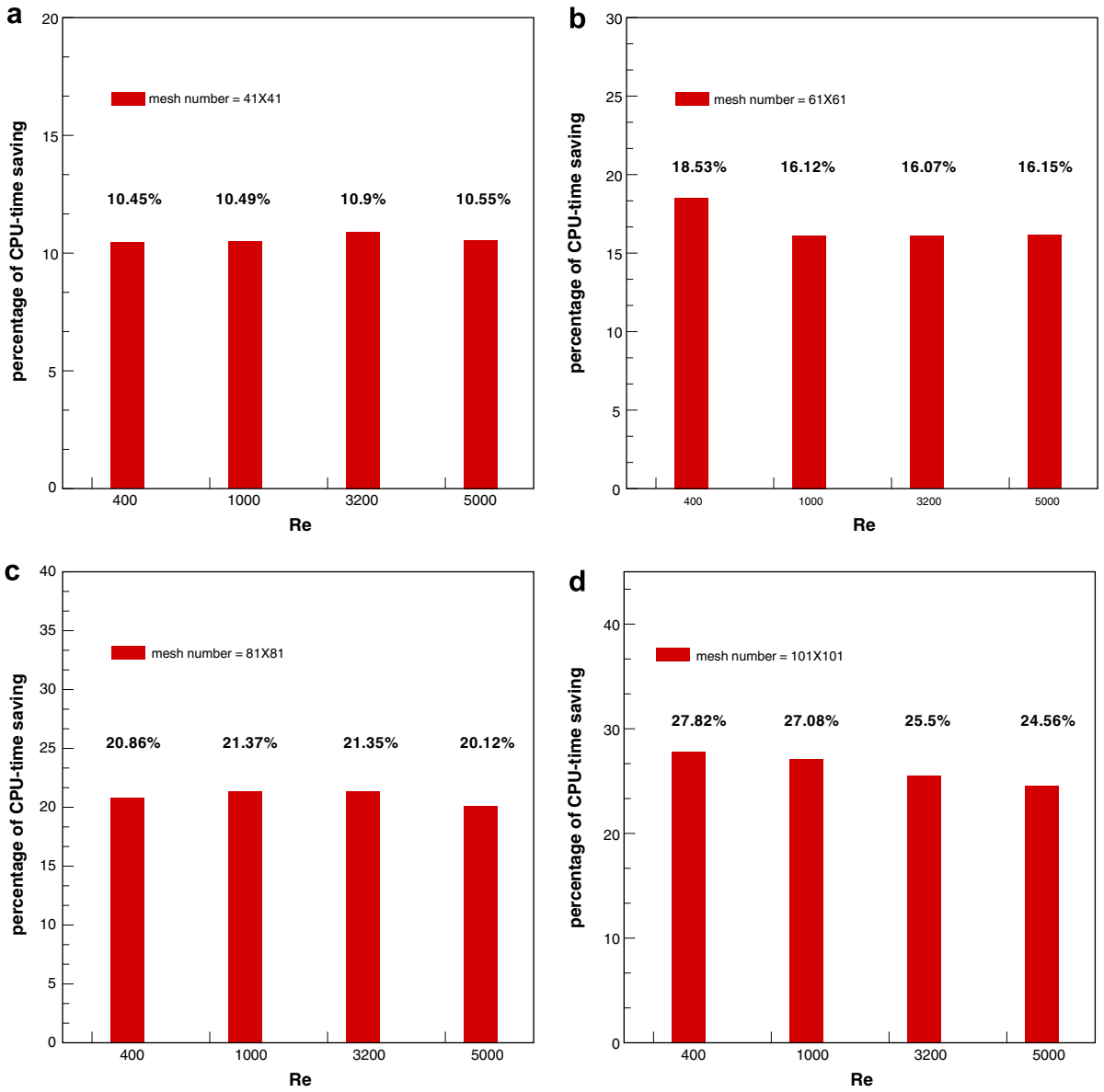

Fig. 12. Comparison of the reduced percentages of the CPU time for the two proposed schemes for approximating ∇p in the non-staggered grids at different Reynolds numbers and mesh points. (a) 41×41; (b) 61×61; (c) 81×81; (d) 101×101.

6. Concluding remarks

The main feature of the two-level method proposed for effectively solving the incompressible Navier–Stokes solutions in non-staggered grids is the derived prolongation operator aimed to accurately communicate the nodal velocities obtained at the grid points in two mesh levels. Another distinct feature of the present scheme development is the transformation of the convection–diffusion differential equation into the convection–diffusion–reaction equation so as to be able to apply the rigorously derived CDR discretization scheme. For the sake of computational efficiency, the pressure gradient term is approximated explicitly using the scheme which can accommodate the essence of the derived implicit DRP compact scheme for ∇p in non-staggered grids without yielding oscillatory pressure solutions. Good agreement

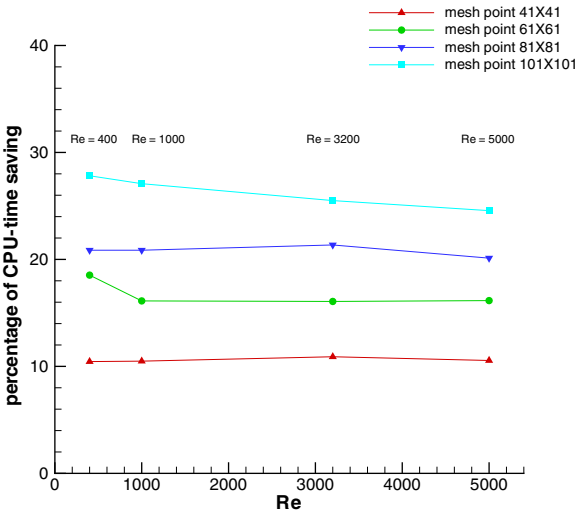

Fig. 13. Comparison of the reduced percentages of the CPU time for the two proposed schemes for approximating ∇p in the non-staggered grids at different Reynolds numbers and mesh points.

between the predicted and analytical solutions is demonstrated for the analytic test problem. The predicted spatial rates of convergence are also shown to be quadratic. In addition, the present study clearly shows that a slight deterioration of the prediction accuracy owing to the use of Oseen-type two-level method accompanies, however, a considerable amount of the CPU time saving due to the largely reduced nonlinear iteration number. The larger the problem size is, the greater amount of the computing time can be saved.

Acknowledgment

This work was supported by the National Science Council of the Republic of China under Grants NSC94-2611-E-002-021 and NSC94-2745-P-002-002.

Appendix

The coefficients $\overline{A_1} \sim \overline{A_4}$ shown in Eq. (8) are summarized below:

$$
\begin{aligned}
\overline{A}_1 = \Big(& -e^{\frac{By3}{K}}\phi_2\, e^{\frac{Ax1}{K}} + e^{\frac{Ax1}{K}} e^{\frac{By4}{K}}\phi_2 - e^{\frac{By4}{K}} e^{\frac{Ax1}{K}}\phi_3 + \phi_3\, e^{\frac{By2}{K}} e^{\frac{Ax1}{K}} + \phi_4\, e^{\frac{Ax1}{K}} e^{\frac{By3}{K}} - e^{\frac{Ax1}{K}}\phi_4\, e^{\frac{By2}{K}} - \phi_1\, e^{\frac{By2}{K}} e^{\frac{Ax3}{K}} \\
& + e^{\frac{By4}{K}} e^{\frac{Ax2}{K}}\phi_3 - \phi_3\, e^{\frac{Ax2}{K}} e^{\frac{By1}{K}} - e^{\frac{By4}{K}} e^{\frac{Ax2}{K}}\phi_1 - \phi_4\, e^{\frac{Ax2}{K}} e^{\frac{By3}{K}} + \phi_4\, e^{\frac{Ax2}{K}} e^{\frac{By1}{K}} + \phi_4 e^{\frac{Ax3}{K}} e^{\frac{By2}{K}} - e^{\frac{Ax4}{K}}\phi_1\, e^{\frac{By3}{K}} + e^{\frac{Ax4}{K}}\phi_1\, e^{\frac{By2}{K}} \\
& + e^{\frac{Ax4}{K}} e^{\frac{By3}{K}}\phi_2 + e^{\frac{Ax4}{K}} e^{\frac{By1}{K}}\phi_3 - e^{\frac{Ax4}{K}} e^{\frac{By1}{K}}\phi_2 + e^{\frac{By3}{K}} e^{\frac{Ax2}{K}}\phi_1 - e^{\frac{By4}{K}} e^{\frac{Ax3}{K}}\phi_2 - e^{\frac{Ax4}{K}}\phi_3\, e^{\frac{By2}{K}} + e^{\frac{By1}{K}}\phi_2\, e^{\frac{Ax3}{K}} - \phi_4\, e^{\frac{Ax3}{K}} e^{\frac{By1}{K}} \\
& + e^{\frac{By4}{K}} e^{\frac{Ax3}{K}}\phi_1 \Big)\Big(e^{\frac{Ax1}{K}} e^{\frac{By3}{K}} e^{\frac{Ax2}{K}} e^{\frac{By1}{K}} + e^{\frac{Ax3}{K}} e^{\frac{By3}{K}} e^{\frac{By2}{K}} e^{\frac{Ax1}{K}} - e^{\frac{By3}{K}} e^{\frac{Ax2}{K}} e^{\frac{By2}{K}} e^{\frac{Ax1}{K}} - e^{\frac{Ax1}{K}} e^{\frac{Ax4}{K}} e^{\frac{By4}{K}} e^{\frac{By2}{K}} - e^{\frac{Ax1}{K}} e^{\frac{By1}{K}} e^{\frac{By2}{K}} e^{\frac{Ax3}{K}} \\
& - e^{\frac{Ax1}{K}} e^{\frac{Ax4}{K}} e^{\frac{By1}{K}} e^{\frac{By3}{K}} + e^{\frac{Ax4}{K}} e^{\frac{By1}{K}} e^{\frac{By2}{K}} e^{\frac{Ax1}{K}} + e^{\frac{By4}{K}} e^{\frac{Ax1}{K}} e^{\frac{Ax3}{K}} e^{\frac{By1}{K}} - e^{\frac{By4}{K}} e^{\frac{Ax1}{K}} e^{\frac{Ax2}{K}} e^{\frac{By1}{K}} + e^{\frac{Ax1}{K}} e^{\frac{By4}{K}} e^{\frac{Ax2}{K}} e^{\frac{By2}{K}} - e^{\frac{By4}{K}} e^{\frac{Ax3}{K}} e^{\frac{By3}{K}} e^{\frac{Ax1}{K}} \\
& + e^{\frac{Ax4}{K}} e^{\frac{By4}{K}} e^{\frac{Ax1}{K}} e^{\frac{By3}{K}} + e^{\frac{By1}{K}} e^{\frac{Ax2}{K}} e^{\frac{By2}{K}} e^{\frac{Ax3}{K}} - e^{\frac{Ax4}{K}} e^{\frac{By3}{K}} e^{\frac{By2}{K}} e^{\frac{Ax3}{K}} + e^{\frac{Ax4}{K}} e^{\frac{By3}{K}} e^{\frac{Ax3}{K}} e^{\frac{By1}{K}} + e^{\frac{Ax4}{K}} e^{\frac{By3}{K}} e^{\frac{Ax2}{K}} e^{\frac{By2}{K}} - e^{\frac{Ax4}{K}} e^{\frac{By1}{K}} e^{\frac{Ax2}{K}} e^{\frac{By2}{K}} \\
& - e^{\frac{By4}{K}} e^{\frac{Ax3}{K}} e^{\frac{Ax2}{K}} e^{\frac{By2}{K}} - e^{\frac{Ax3}{K}} e^{\frac{By1}{K}} e^{\frac{Ax2}{K}} e^{\frac{By3}{K}} + e^{\frac{Ax4}{K}} e^{\frac{By4}{K}} e^{\frac{Ax3}{K}} e^{\frac{By2}{K}} - e^{\frac{Ax4}{K}} e^{\frac{By4}{K}} e^{\frac{Ax2}{K}} e^{\frac{By3}{K}} + e^{\frac{Ax4}{K}} e^{\frac{By4}{K}} e^{\frac{Ax2}{K}} e^{\frac{By1}{K}} - e^{\frac{Ax4}{K}} e^{\frac{By4}{K}} e^{\frac{Ax3}{K}} e^{\frac{By1}{K}} \\
& + e^{\frac{By4}{K}} e^{\frac{Ax3}{K}} e^{\frac{Ax2}{K}} e^{\frac{By3}{K}} \Big)^{-1},
\end{aligned}
$$

$$
\begin{aligned}
\overline{A}_2 = &-\Big(e^{\frac{By1}{K}} e^{\frac{Ax1}{K}} \phi_3\, e^{\frac{By2}{K}} - e^{\frac{Ax1}{K}} \phi_2\, e^{\frac{By1}{K}} e^{\frac{By3}{K}} + e^{\frac{By1}{K}} e^{\frac{Ax1}{K}} \phi_2\, e^{\frac{By4}{K}} - e^{\frac{By1}{K}} e^{\frac{Ax1}{K}} \phi_3\, e^{\frac{By4}{K}} + e^{\frac{Ax1}{K}} e^{\frac{By1}{K}} \phi_4\, e^{\frac{By3}{K}} - e^{\frac{By1}{K}} e^{\frac{Ax1}{K}} \phi_4\, e^{\frac{By2}{K}} \\
&+ e^{\frac{By3}{K}} e^{\frac{Ax3}{K}} \phi_1\, e^{\frac{By4}{K}} - e^{\frac{By3}{K}} e^{\frac{Ax3}{K}} \phi_2\, e^{\frac{By4}{K}} - \phi_3 e^{\frac{Ax4}{K}} e^{\frac{By4}{K}}\, e^{\frac{By2}{K}} + e^{\frac{By3}{K}} e^{\frac{By1}{K}} e^{\frac{Ax3}{K}} \phi_2 - e^{\frac{By3}{K}} e^{\frac{By1}{K}}\, e^{\frac{Ax3}{K}} \phi_4 + e^{\frac{By3}{K}} \phi_2\, e^{\frac{Ax4}{K}} e^{\frac{By4}{K}} \\
&- e^{\frac{By3}{K}} e^{\frac{Ax3}{K}} \phi_1\, e^{\frac{By2}{K}} + e^{\frac{By3}{K}}\, e^{\frac{Ax3}{K}} e^{\frac{By2}{K}} \phi_4 + \phi_1\, e^{\frac{Ax4}{K}} e^{\frac{By4}{K}} e^{\frac{By2}{K}} - \phi_1\, e^{\frac{Ax4}{K}} e^{\frac{By4}{K}}\, e^{\frac{By3}{K}} + e^{\frac{Ax2}{K}} \phi_3\, e^{\frac{By4}{K}} e^{\frac{By2}{K}} - e^{\frac{Ax2}{K}} \phi_1\, e^{\frac{By4}{K}} e^{\frac{By2}{K}} \\
&- e^{\frac{By3}{K}} e^{\frac{Ax2}{K}} \phi_4 e^{\frac{By2}{K}} - e^{\frac{By1}{K}} \phi_3\, e^{\frac{Ax2}{K}} e^{\frac{By2}{K}} + e^{\frac{By1}{K}} \phi_3\, e^{\frac{Ax4}{K}} e^{\frac{By4}{K}} - e^{\frac{By1}{K}} \phi_2 e^{\frac{Ax4}{K}} e^{\frac{By4}{K}} + e^{\frac{By1}{K}} e^{\frac{Ax2}{K}} \phi_4\, e^{\frac{By2}{K}} + e^{\frac{Ax2}{K}}\, e^{\frac{By2}{K}} \phi_1\, e^{\frac{By3}{K}} \Big) \\
&\times \Big(e^{\frac{Ax1}{K}} e^{\frac{By3}{K}}\, e^{\frac{Ax2}{K}} e^{\frac{By1}{K}} + e^{\frac{Ax3}{K}} e^{\frac{By3}{K}}\, e^{\frac{By2}{K}} e^{\frac{Ax1}{K}} - e^{\frac{By3}{K}} e^{\frac{Ax2}{K}}\, e^{\frac{By2}{K}} e^{\frac{Ax1}{K}} - e^{\frac{Ax1}{K}} e^{\frac{Ax4}{K}} e^{\frac{By4}{K}} e^{\frac{By2}{K}} - e^{\frac{Ax1}{K}} e^{\frac{By1}{K}}\, e^{\frac{By2}{K}} e^{\frac{Ax3}{K}} \\
&- e^{\frac{Ax1}{K}} e^{\frac{Ax4}{K}}\, e^{\frac{By1}{K}} e^{\frac{By3}{K}} + e^{\frac{Ax4}{K}} e^{\frac{By1}{K}}\, e^{\frac{By2}{K}} e^{\frac{Ax1}{K}} + e^{\frac{By4}{K}} e^{\frac{Ax1}{K}}\, e^{\frac{Ax3}{K}} e^{\frac{By1}{K}} - e^{\frac{By4}{K}} e^{\frac{Ax1}{K}}\, e^{\frac{Ax2}{K}} e^{\frac{By1}{K}} + e^{\frac{Ax1}{K}} e^{\frac{By4}{K}}\, e^{\frac{Ax2}{K}} e^{\frac{By2}{K}} \\
&- e^{\frac{By4}{K}} e^{\frac{Ax3}{K}}\, e^{\frac{By3}{K}} e^{\frac{Ax1}{K}} + e^{\frac{Ax4}{K}} e^{\frac{By4}{K}} e^{\frac{Ax1}{K}} e^{\frac{By3}{K}} + e^{\frac{By1}{K}} e^{\frac{Ax2}{K}}\, e^{\frac{By2}{K}} e^{\frac{Ax3}{K}} - e^{\frac{Ax4}{K}} e^{\frac{By3}{K}}\, e^{\frac{By2}{K}} e^{\frac{Ax3}{K}} + e^{\frac{Ax4}{K}} e^{\frac{By3}{K}}\, e^{\frac{Ax3}{K}} e^{\frac{By1}{K}} \\
&+ e^{\frac{Ax4}{K}} e^{\frac{By3}{K}}\, e^{\frac{Ax2}{K}} e^{\frac{By2}{K}} - e^{\frac{Ax4}{K}} e^{\frac{By1}{K}}\, e^{\frac{Ax2}{K}} e^{\frac{By2}{K}} - e^{\frac{By4}{K}} e^{\frac{Ax3}{K}}\, e^{\frac{Ax2}{K}} e^{\frac{By2}{K}} - e^{\frac{Ax3}{K}} e^{\frac{By1}{K}}\, e^{\frac{Ax2}{K}} e^{\frac{By3}{K}} + e^{\frac{Ax4}{K}} e^{\frac{By4}{K}} e^{\frac{Ax3}{K}} e^{\frac{By2}{K}} \\
&- e^{\frac{Ax4}{K}} e^{\frac{By4}{K}}\, e^{\frac{Ax2}{K}} e^{\frac{By3}{K}} + e^{\frac{Ax4}{K}} e^{\frac{By4}{K}}\, e^{\frac{Ax2}{K}} e^{\frac{By1}{K}} - e^{\frac{Ax4}{K}} e^{\frac{By4}{K}}\, e^{\frac{Ax3}{K}} e^{\frac{By1}{K}} + e^{\frac{By4}{K}} e^{\frac{Ax3}{K}}\, e^{\frac{Ax2}{K}} e^{\frac{By3}{K}} \Big)^{-1},
\end{aligned}
$$

$$
\begin{aligned}
\overline{A}_3 = &-\Big(e^{\frac{By1}{K}} e^{\frac{Ax3}{K}}\, e^{\frac{Ax1}{K}} \phi_2 - e^{\frac{By1}{K}}\, e^{\frac{Ax3}{K}} e^{\frac{Ax1}{K}} \phi_4 + e^{\frac{By1}{K}} e^{\frac{Ax1}{K}} \phi_3\, e^{\frac{Ax4}{K}} + e^{\frac{By1}{K}}\, e^{\frac{Ax1}{K}} \phi_4 e^{\frac{Ax2}{K}} - e^{\frac{By1}{K}} e^{\frac{Ax1}{K}} \phi_2 e^{\frac{Ax4}{K}} \\
&- e^{\frac{By1}{K}} e^{\frac{Ax1}{K}} \phi_3\, e^{\frac{Ax2}{K}} - e^{\frac{Ax3}{K}}\, e^{\frac{By3}{K}} \phi_2\, e^{\frac{Ax1}{K}} + e^{\frac{Ax3}{K}} \phi_1\, e^{\frac{Ax4}{K}} e^{\frac{By4}{K}} - e^{\frac{Ax3}{K}} e^{\frac{Ax4}{K}} \phi_1\, e^{\frac{By3}{K}} - e^{\frac{Ax3}{K}} \phi_4\, e^{\frac{Ax2}{K}} e^{\frac{By3}{K}} \\
&- e^{\frac{Ax3}{K}} \phi_1 e^{\frac{Ax2}{K}}\, e^{\frac{By2}{K}} + e^{\frac{Ax3}{K}} \phi_4\, e^{\frac{Ax1}{K}} e^{\frac{By3}{K}} + e^{\frac{Ax3}{K}} e^{\frac{By3}{K}}\, e^{\frac{Ax2}{K}} \phi_1 + e^{\frac{Ax3}{K}}\, e^{\frac{Ax2}{K}} e^{\frac{By2}{K}} \phi_4 + e^{\frac{Ax3}{K}} e^{\frac{Ax4}{K}}\, e^{\frac{By3}{K}} \phi_2 \\
&- e^{\frac{Ax3}{K}} \phi_2 e^{\frac{Ax4}{K}}\, e^{\frac{By4}{K}} + e^{\frac{Ax1}{K}} \phi_3\, e^{\frac{Ax2}{K}} e^{\frac{By2}{K}} - e^{\frac{Ax1}{K}} \phi_3 e^{\frac{Ax4}{K}}\, e^{\frac{By4}{K}} - e^{\frac{Ax2}{K}} \phi_1 e^{\frac{Ax4}{K}} e^{\frac{By4}{K}} + e^{\frac{Ax1}{K}} \phi_2\, e^{\frac{Ax4}{K}} e^{\frac{By4}{K}} + e^{\frac{Ax2}{K}} \phi_3 e^{\frac{Ax4}{K}}\, e^{\frac{By4}{K}} \\
&+ e^{\frac{Ax2}{K}} \phi_1\, e^{\frac{Ax4}{K}} e^{\frac{By2}{K}} - e^{\frac{Ax2}{K}} \phi_3 e^{\frac{Ax4}{K}}\, e^{\frac{By2}{K}} - e^{\frac{Ax1}{K}}\, e^{\frac{Ax2}{K}} \phi_4 e^{\frac{By2}{K}} \Big) \Big(e^{\frac{Ax1}{K}} e^{\frac{By3}{K}}\, e^{\frac{Ax2}{K}} e^{\frac{By1}{K}} + e^{\frac{Ax3}{K}} e^{\frac{By3}{K}}\, e^{\frac{By2}{K}} e^{\frac{Ax1}{K}} \\
&- e^{\frac{By3}{K}} e^{\frac{Ax2}{K}}\, e^{\frac{By2}{K}} e^{\frac{Ax1}{K}} - e^{\frac{Ax1}{K}} e^{\frac{Ax4}{K}}\, e^{\frac{By4}{K}} e^{\frac{By2}{K}} - e^{\frac{Ax1}{K}} e^{\frac{By1}{K}}\, e^{\frac{By2}{K}} e^{\frac{Ax3}{K}} - e^{\frac{Ax1}{K}} e^{\frac{Ax4}{K}}\, e^{\frac{By1}{K}} e^{\frac{By3}{K}} + e^{\frac{Ax4}{K}} e^{\frac{By1}{K}}\, e^{\frac{By2}{K}} e^{\frac{Ax1}{K}} \\
&+ e^{\frac{By4}{K}} e^{\frac{Ax1}{K}}\, e^{\frac{Ax3}{K}} e^{\frac{By1}{K}} - e^{\frac{By4}{K}} e^{\frac{Ax1}{K}}\, e^{\frac{Ax2}{K}} e^{\frac{By1}{K}} + e^{\frac{Ax1}{K}} e^{\frac{By4}{K}}\, e^{\frac{Ax2}{K}} e^{\frac{By2}{K}} - e^{\frac{By4}{K}} e^{\frac{Ax3}{K}}\, e^{\frac{By3}{K}} e^{\frac{Ax1}{K}} + e^{\frac{Ax4}{K}} e^{\frac{By4}{K}}\, e^{\frac{Ax1}{K}} e^{\frac{By3}{K}} \\
&+ e^{\frac{By1}{K}} e^{\frac{Ax2}{K}}\, e^{\frac{By2}{K}} e^{\frac{Ax3}{K}} - e^{\frac{Ax4}{K}} e^{\frac{By3}{K}}\, e^{\frac{By2}{K}} e^{\frac{Ax3}{K}} + e^{\frac{Ax4}{K}} e^{\frac{By3}{K}}\, e^{\frac{Ax3}{K}} e^{\frac{By1}{K}} + e^{\frac{Ax4}{K}} e^{\frac{By3}{K}}\, e^{\frac{Ax2}{K}} e^{\frac{By2}{K}} - e^{\frac{Ax4}{K}} e^{\frac{By1}{K}}\, e^{\frac{Ax2}{K}} e^{\frac{By2}{K}} \\
&- e^{\frac{By4}{K}} e^{\frac{Ax3}{K}}\, e^{\frac{Ax2}{K}} e^{\frac{By2}{K}} - e^{\frac{Ax3}{K}} e^{\frac{By1}{K}}\, e^{\frac{Ax2}{K}} e^{\frac{By3}{K}} + e^{\frac{Ax4}{K}} e^{\frac{By4}{K}} e^{\frac{Ax3}{K}} e^{\frac{By2}{K}} - e^{\frac{Ax4}{K}} e^{\frac{By4}{K}}\, e^{\frac{Ax2}{K}} e^{\frac{By3}{K}} + e^{\frac{Ax4}{K}} e^{\frac{By4}{K}}\, e^{\frac{Ax2}{K}} e^{\frac{By1}{K}} \\
&- e^{\frac{Ax4}{K}} e^{\frac{By4}{K}}\, e^{\frac{Ax3}{K}} e^{\frac{By1}{K}} + e^{\frac{By4}{K}} e^{\frac{Ax3}{K}}\, e^{\frac{Ax2}{K}} e^{\frac{By3}{K}} \Big)^{-1},
\end{aligned}
$$

$$
\begin{aligned}
\overline{A}_4 = &\Big(e^{\frac{Ax1}{K}} e^{\frac{By1}{K}}\, e^{\frac{Ax4}{K}} \phi_3 e^{\frac{By2}{K}} + e^{\frac{Ax3}{K}} e^{\frac{By3}{K}}\, e^{\frac{Ax1}{K}} \phi_4 e^{\frac{By2}{K}} - e^{\frac{Ax3}{K}} e^{\frac{By3}{K}}\, e^{\frac{Ax4}{K}} \phi_1 e^{\frac{By2}{K}} + e^{\frac{Ax1}{K}} \phi_2 e^{\frac{By4}{K}}\, e^{\frac{Ax3}{K}} e^{\frac{By1}{K}} + e^{\frac{Ax3}{K}} \phi_1\, e^{\frac{By4}{K}} e^{\frac{Ax2}{K}}\, e^{\frac{By3}{K}} \\
&- \phi_3\, e^{\frac{Ax1}{K}} e^{\frac{Ax4}{K}}\, e^{\frac{By4}{K}} e^{\frac{By2}{K}} + e^{\frac{By3}{K}} e^{\frac{By1}{K}}\, e^{\frac{Ax1}{K}} \phi_4\, e^{\frac{Ax2}{K}} - e^{\frac{By3}{K}} e^{\frac{By1}{K}} e^{\frac{Ax1}{K}} \phi_2 e^{\frac{Ax4}{K}} - e^{\frac{By3}{K}} e^{\frac{Ax2}{K}} \phi_1\, e^{\frac{Ax4}{K}} e^{\frac{By4}{K}} + e^{\frac{By3}{K}} e^{\frac{Ax1}{K}} \phi_2\, e^{\frac{Ax4}{K}} e^{\frac{By4}{K}} \\
&+ \phi_1\, e^{\frac{Ax4}{K}} e^{\frac{By4}{K}} e^{\frac{Ax3}{K}} e^{\frac{By2}{K}} - e^{\frac{Ax1}{K}} \phi_3 e^{\frac{By4}{K}}\, e^{\frac{Ax2}{K}} e^{\frac{By1}{K}} - e^{\frac{Ax2}{K}} \phi_1 e^{\frac{By4}{K}}\, e^{\frac{Ax3}{K}} e^{\frac{By2}{K}} + e^{\frac{Ax2}{K}} \phi_3\, e^{\frac{Ax1}{K}} e^{\frac{By4}{K}}\, e^{\frac{By2}{K}} + e^{\frac{By3}{K}} e^{\frac{Ax2}{K}} \phi_1 e^{\frac{Ax4}{K}}\, e^{\frac{By2}{K}} \\
&- e^{\frac{By3}{K}}\, e^{\frac{Ax1}{K}} e^{\frac{Ax2}{K}} \phi_4\, e^{\frac{By2}{K}} - e^{\frac{By1}{K}} e^{\frac{Ax3}{K}} \phi_4\, e^{\frac{Ax2}{K}} e^{\frac{By3}{K}} + e^{\frac{By1}{K}} e^{\frac{Ax3}{K}}\, e^{\frac{Ax2}{K}} e^{\frac{By2}{K}} \phi_4 + e^{\frac{By1}{K}} e^{\frac{Ax3}{K}}\, e^{\frac{Ax4}{K}} e^{\frac{By3}{K}} \phi_2 - e^{\frac{By1}{K}} e^{\frac{Ax3}{K}} \phi_2\, e^{\frac{Ax4}{K}} e^{\frac{By4}{K}} \\
&+ e^{\frac{By1}{K}} e^{\frac{Ax2}{K}} \phi_3\, e^{\frac{Ax4}{K}} e^{\frac{By4}{K}} - e^{\frac{By1}{K}} e^{\frac{Ax2}{K}} \phi_3 e^{\frac{Ax4}{K}} e^{\frac{By2}{K}} - e^{\frac{Ax1}{K}} e^{\frac{By1}{K}} \phi_4\, e^{\frac{Ax3}{K}} e^{\frac{By2}{K}} - e^{\frac{Ax3}{K}} \phi_2 e^{\frac{By4}{K}}\, e^{\frac{Ax1}{K}} e^{\frac{By3}{K}} \Big) \\
&\times \Big(e^{\frac{Ax1}{K}} e^{\frac{By3}{K}}\, e^{\frac{Ax2}{K}} e^{\frac{By1}{K}} + e^{\frac{Ax3}{K}} e^{\frac{By3}{K}}\, e^{\frac{By2}{K}} e^{\frac{Ax1}{K}} - e^{\frac{By3}{K}} e^{\frac{Ax2}{K}}\, e^{\frac{By2}{K}} e^{\frac{Ax1}{K}} - e^{\frac{Ax1}{K}} e^{\frac{Ax4}{K}}\, e^{\frac{By4}{K}} e^{\frac{By2}{K}} - e^{\frac{Ax1}{K}} e^{\frac{By1}{K}}\, e^{\frac{By2}{K}} e^{\frac{Ax3}{K}} \\
&- e^{\frac{Ax1}{K}} e^{\frac{Ax4}{K}} e^{\frac{By1}{K}} e^{\frac{By3}{K}} + e^{\frac{Ax4}{K}} e^{\frac{By1}{K}}\, e^{\frac{By2}{K}} e^{\frac{Ax1}{K}} + e^{\frac{By4}{K}} e^{\frac{Ax1}{K}}\, e^{\frac{Ax3}{K}} e^{\frac{By1}{K}} - e^{\frac{By4}{K}} e^{\frac{Ax1}{K}}\, e^{\frac{Ax2}{K}} e^{\frac{By1}{K}} + e^{\frac{Ax1}{K}} e^{\frac{By4}{K}}\, e^{\frac{Ax2}{K}} e^{\frac{By2}{K}} \\
&- e^{\frac{By4}{K}} e^{\frac{Ax3}{K}}\, e^{\frac{By3}{K}} e^{\frac{Ax1}{K}} + e^{\frac{Ax4}{K}} e^{\frac{By4}{K}}\, e^{\frac{Ax1}{K}} e^{\frac{By3}{K}} + e^{\frac{By1}{K}} e^{\frac{Ax2}{K}}\, e^{\frac{By2}{K}} e^{\frac{Ax3}{K}} - e^{\frac{Ax4}{K}} e^{\frac{By3}{K}} e^{\frac{By2}{K}} e^{\frac{Ax3}{K}} + e^{\frac{Ax4}{K}} e^{\frac{By3}{K}}\, e^{\frac{Ax3}{K}} e^{\frac{By1}{K}} + e^{\frac{Ax4}{K}} e^{\frac{By3}{K}}\, e^{\frac{Ax2}{K}} e^{\frac{By2}{K}} \\
&- e^{\frac{Ax4}{K}} e^{\frac{By1}{K}}\, e^{\frac{Ax2}{K}} e^{\frac{By2}{K}} - e^{\frac{By4}{K}} e^{\frac{Ax3}{K}}\, e^{\frac{Ax2}{K}} e^{\frac{By2}{K}} - e^{\frac{Ax3}{K}} e^{\frac{By1}{K}}\, e^{\frac{Ax2}{K}} e^{\frac{By3}{K}} + e^{\frac{Ax4}{K}} e^{\frac{By4}{K}} e^{\frac{Ax3}{K}} e^{\frac{By2}{K}} - e^{\frac{Ax4}{K}} e^{\frac{By4}{K}}\, e^{\frac{Ax2}{K}} e^{\frac{By3}{K}} \\
&+ e^{\frac{Ax4}{K}} e^{\frac{By4}{K}} e^{\frac{Ax2}{K}} e^{\frac{By1}{K}} - e^{\frac{Ax4}{K}} e^{\frac{By4}{K}}\, e^{\frac{Ax3}{K}} e^{\frac{By1}{K}} + e^{\frac{By4}{K}} e^{\frac{Ax3}{K}}\, e^{\frac{Ax2}{K}} e^{\frac{By3}{K}} \Big)^{-1}.
\end{aligned}
$$

References

[1] S.V. Patankar, Numerical Heat Transfer and Fluid Flow, Hemisphere, New York, 1980.
[2] Tony W.H. Sheu, S.K. Wang, R.K. Lin, An implicit scheme for solving the convection–diffusion–reaction equation in two dimensions, J. Comput. Phys. 164 (2000) 123–142.
[3] C.M. Rhie, W.L. Chow, A numerical study of the turbulent flow past an airfoil with trailling edge separation, AIAA J. 21 (1983) 1525–1532.
[4] S.W. Armfield, Finite difference solutions of the Navier–Stokes equations on staggered and non-staggered grids, Comput. Fluids 20 (1991) 1–17.
[5] A.W. Date, Solution of Navier–Stokes equations on non-staggered grids, Int. J. Heat Mass Transfer 36 (1993) 1913–1922.
[6] I.E. Barton, R. Kirby, Finite difference scheme for the solution of fluid flow problems on non-staggered grids, Int. J. Numer. Methods Fluids 33 (2000) 939–959.
[7] W. Layton, A two-level discretization method for the Navier–Stokes equations, Comput. Math. Appl. 26 (1993) 33–38.
[8] W. Layton, W. Lenferink, Two-level Picard and modified Picard methods for the Navier–Stokes equations, Appl. Math. Comput. 69 (1995) 263–274.
[9] L. Quartapelle, M. Napolitano, Integral conditions for the pressure in the computation of incompressible viscous flows, J. Comput. Phys. 64 (1986) 340–348.
[10] M.M.T. Wang, Tony W.H. Sheu, An element-by-element BICGSTAB iterative method for three-dimensional steady Navier–Stokes equations, J. Comput. Appl. Math. 79 (1997) 147–165.
[11] P.M. Gresho, R.L. Sani, On pressure boundary conditions for the incompressible Navier–Stokes equations, Int. J. Numer. Methods Fluids 7 (1987) 1111–1145.
[12] S. Turek, A comparative study of time-stepping techniques for the incompressible Navier–Stokes equations: from fully implicit non-linear schemes to semi-implicit methods, Int. J. Numer. Methods Fluids 22 (1996) 987–1011.
[13] J. Xu, A novel two-grid method for semilinear elliptic equations, SIAM J. Sci. Comput. 15 (1994) 231–237.
[14] J. Xu, Two-grid finite element discretizations for nonlinear PDE's, SIAM J. Numer. Anal. 33 (1996) 1759–1777.
[15] L. Wu, M.B. Allen, A two-grid method for mixed finite-element solution of reaction–diffusion equations, Numer. Methods Partial Differen. Equat. 15 (1999) 317–332.
[16] V. Girault, P.A. Raviart, Finite element methods for the Navier–Stokes equations, Theory and Algorithms, Springer Ser. Comput. Math., vol. 5, Springer-Verlag, Berlin, 1986.
[17] C. Lin, J. Liu, S. McCormick, Multilevel adaptive methods for incompressible flow in grooved channels, J. Comput. Appl. Math. 38 (1991) 283–295.
[18] W. Layton, L. Tobiska, A two-level method with backtracking for the Navier–Stokes equations, SIAM J. Numer. Anal. 35 (1998) 2035–2054.
[19] Tony W.H. Sheu, R.K. Lin, An incompressible Navier–Stokes model implemented on non-staggered grids, Numer. Heat Transfer B, Fundam. 44 (2003) 277–294.
[20] C.K.W. Tam, J.C. Webb, Dispersion-relation-preserving finite difference schemes for computational acoustics, J. Comput. Phys. 107 (1992) 262–281.
[21] I.A. Abalakin, A.V. Alexandrov, V.G. Bobkov, T.K. Kozubskaya, High accuracy methods and software development in computational aeroacoustics, J. Comput. Methods Sci. Eng. 2 (2003) 1–14.
[22] F.Q. Hu, M.Y. Hussaini, J.L. Manthey, Low-dissipation and low-dispersion Runge–Kutta schemes for computational acoustics, J. Comput. Phys. 124 (1996) 177–191.
[23] C. Bogry, C. Bailly, A family of low dispersive and low dissipative explicit schemes for flow and noise computations, J. Comput. Phys. 194 (2004) 194–214.
[24] T.K. Sengupta, G. Ganeriwal, S. De, Analysis of central and upwind compact schemes, J. Comput. Phys. 192 (2003) 677–694.
[25] J.W. Kim, D.J. Lee, Optimized compact finite difference schemes with maximum resolution, AIAA J. 34 (1996) 887–893.
[26] G. Ashcroft, X. Zhang, Optimized prefactored compact schemes, J. Comput. Phys. 190 (2003) 459–477.
[27] P.H. Chiu, Tony W.H. Sheu, R.K. Lin, Development of a dispersion-relation-preserving upwinding scheme for incompressible Navier–Stokes equations on non-staggered grids, Numer. Heat Transfer B, Fundam. 48 (2005) 543–569.
[28] S.K. Lele, Compact finite difference schemes with spectral-like resolution, J. Comput. Phys. 103 (1992) 16–42.
[29] U. Ghia, K.N. Ghia, C.T. Shin, High-Re solutions for incompressible flow using the Navier–Stokes equations and a multigrid method, J. Comput. Phys. 48 (1982) 387–411.
[30] E. Erturk, T.C. Corke, C. Gökcöl, Numerical solutions of 2D steady incompressible driven cavity flow at high Reynolds numbers, Int. J. Numer. Methods Fluids 48 (2005) 747–774.